2005-07-11

Effects of Hurricane Fault Architecture on Groundwater Flow in the Timpoweap Canyon of Southwestern, Utah

Sarah J. Dutson
Brigham Young University - Provo

EFFECTS OF HURRICANE FAULT ARCHITECTURE ON GROUNDWATER FLOW IN THE TIMPOWEAP CANYON OF SOUTHWESTERN, UTAH

By

Sarah Janeen Dutson

A thesis submitted to the faculty of

Brigham Young University

in partial fulfillment of the requirements for the degree of

Master of Science

Department of Geology

Brigham Young University

August 2005

BRIGHAM YOUNG UNIVERSITY

GRADUATE COMMITTEE APPROVAL

of a thesis submitted by

Sarah Janeen Dutson

This thesis has been read by each member of the following graduate committee and by majority vote has been found to be satisfactory.

Date	Alan L. Mayo, Committee Chair
Date	Stephen T. Nelson
Date	Ron A. Harris

BRIGHAM YOUNG UNIVERSITY

As chair of the candidate's graduate committee, I have read the thesis of Sarah Janeen Dutson in its final form and have found that (1) its format, citations, and bibliographical style are consistent and acceptable and fulfill the university and department style requirements; (2) its illustrative materials including figures, tables, and charts are in place; and (3) the final manuscript is satisfactory to the graduate committee and is ready for submission to the university library.

_____
Date

_____
Alan L. Mayo
Chair, Graduate Committee

Accepted for the Department

_____
Bart J. Kowallis
Graduate Coordinator

Accepted for the College

_____
G. Rex Bryce
Associate Dean, College of
Physical and Mathematical Sciences

ABSTRACT

EFFECTS OF HURRICANE FAULT ARCHITECTURE ON
GROUNDWATER FLOW IN THE TIMPOWEAP
CANYON OF SOUTHWESTERN, UTAH

Sarah Janeen Dutson

Department of Geology

Master of Science

Hydrogeologically important features of fault zones include undamaged country rock, the damage zone, and the core zone. Fault cores generally have low porosity and permeability, and often act as a barrier to groundwater flow. The damage zone, by contrast, consists of small faults and fracture networks, which can act as conduits. Timpoweap Canyon near Hurricane, Utah has superb exposures of the fault core and damage zone of the Hurricane Fault. Also within the canyon, springs discharge from the damage zone into the Virgin River, providing an ideal natural laboratory for the study of groundwater discharge from a fault zone.

The Hurricane fault is an active, steeply dipping, normal fault that is 250 km long, and exhibits about 2500 m of displacement. The damage zone in Timpoweap Canyon controls thermal groundwater (~40˚C) and CO_2 gas discharge from highly fractured

limestone. Total spring discharge is 260 L/s. Approximately 4 L/s of CO_2 gas also discharges with the springs. The δ^2H and $\delta^{16}O$ composition of the springs exhibits a geothermal shift from the global meteoric waterline. This suggests that the circulation depth is about 3 km below the ground surface (bgs) in basement bedrock. The CO_2 gas discharging originates from either magmatic sources or from diagenesis. The fracture density in a typical damage zone decreases with increasing distance from the fault, thus spring discharge should also decrease with increasing distance from the fault. The damage zone in Timpoweap Canyon does not follow this pattern because pre-existing fractures that developed from Laramide and Sevier Orogeny stresses suppress the pattern. Collapse structures from gypsum dissolution and large fractures also control the location of spring discharge.

ACKNOWLEDGEMENTS

I would like to thank Ken Anderson for allowing access to the Pah Tempe Springs. I would also like to thank Dr. Alan Mayo for the initial idea for this project and continual guidance and patience through the research and revisions of this thesis. Thanks also go to Dr. Steve Nelson and Dr. Ron Harris for their time spent on this research project. I would especially like to acknowledge Dave Tingey and his son for helping with the surveying and Dave Tingey, Michelle Bushman, and Dave Alderks for help with isotope and solute analysis. I would like to thank those who assisted me with field work: Julia Haroldsen, Teagan Tomlin, Ryan Dutson, Sarah Flint, Amber Johnstun, and Camille Durrant. Thanks go to Marge Morgan and Kris Mortensen for their help and support. I would like to thank Kim Sullivan for computer support and recovery of lost files. I am grateful for my parents and siblings for their support throughout this project.

TABLE OF CONTENTS

LIST OF TABLES

LIST OF FIGURES

INTRODUCTION

Faults greatly impact fluid flow through rocks. Fault zones can be divided into three structural and hydrologic distinct regions (Figure 1): a core zone, a damage zone, and undamaged rock (Caine et al., 1996; Evans et al., 1997). The core zone typically has the lowest porosity and permeability and is composed of fault breccia and gouge. The damage zone is commonly the most permeable zone and consists of small faults and fracture networks of various dimensions. Structural heterogeneity and hydrologic anisotropy of the fault zone depend on the size, shape, and maturity of the fault; width of the damage zone; and fracture density, connectivity, and aperture (Caine et al., 1996; Evans et al., 1997, Gudmundsson, 2001; Harris et al., 2002; Rawling et. al., 2001).

At the Timpoweap Canyon, near Hurricane, Utah, the footwall of the Hurricane fault has superb exposures of a ~200 m wide core and ~500 m wide damage zone (Figure 2). This makes it an excellent location to examine the controls of fault architecture on groundwater flow. The canyon walls are 120 to 240 m high and the canyon floor is 50 to 80 m wide.

The Hurricane fault is an active, steeply west-dipping normal fault, separating the Colorado Plateau from the Basin and Range province (Taylor et al, 2001 and Stewart et al, 1997). CO_2 gas and about 260 L/s of thermal groundwater (~ 40ºC) discharge from the footwall of the fault into the Virgin River in Timpoweap Canyon. These springs are known as the Pah Tempe Hot Springs, La Verkin Hot Springs, or the Dixie Springs.

One model for the source of the Pah Tempe Springs proposed deeply circulating water that is heated magmatically and travels vertically through the highly fractured damage zone of the Hurricane Fault (Mundorff, 1970; U.S. Bureau of Reclamation,

1974). Everittt and Einert (1994) showed the water being heated just by deep circulation and mixing with the Virgin River water near the surface. Stewart et al. (1997) and Taylor et al. (2001) studied neotectonics and fault segmentation of the Hurricane Fault. These studies, however, have not addressed the structural effects of the fault zone on the hydrology of the canyon, nor the origin of the CO_2 gas or the depth of circulation of the water.

PURPOSE AND OBJECTIVES

The purpose of this study is to evaluate the hydrologic properties of the damage zone of the Hurricane fault in Timpoweap Canyon, UT. The specific objectives are:

1. To analyze the orientation, aperture, connectivity and density in the damage zone.
2. To determine possible recharge and depth of circulation of the spring water
3. To determine possible origins of the CO_2 evolving spring water
4. To characterize the movement of groundwater flow in the damage zone,

METHODS OF STUDY

DATA COLLECTION

Flow of the Virgin River in Timpoweap Canyon can vary because of storm events and releases from the Quail Creek Diversion Dam, approximately 3.2 km upstream of the springs. Gain-loss flow measurements of the Virgin River were made during low flow periods using a Flo-Mate portable flowmeter. Flow measurements were taken on three separate days during 2003: March 31, May 14, and May 22. Spring and gain-loss flow measurement locations were determined using a Sokkia SET3E Total Station and standard surveying methods. Survey measurements were based on a north-south grid

system referenced to a temporary bench mark (TBM) (x = 305m, y = 305m, and z = 30m) located near the Pah Tempe Springs. The TBM has a Universal Transverse Mercator (UTM) location of N4118002.47, E298647.54 and an elevation approximately 937 meters above sea level.

Both the number of gas vent outflows and the volume of gas released were estimated. The number of gas vents was counted in surveyed 6.1-meter intervals along the bed of the Virgin River. Intervals extended from the eastern trace of the Hurricane fault to ~525 meters upstream, the location of the eastern most gas vent. The volumes of the gas vent outflows along the streambed were measured using a funnel and a 50-milliliter container. The container and funnel were filled with water, which were then placed over the gas outflows, and the time for the water to be replaced by gas was recorded. The total volume of gas discharge was determined by multiplying the rate by the number of areas of similar size as the area measured by the funnel.

Water samples were collected for solutes and δ^2H and $\delta^{18}O$. Temperature, pH, and conductivity were recorded at sample locations. A sample from the gas vents in the Virgin River was collected on April 3, 2003. The sample was collected following standard gas sampling techniques in a sealed glass bottle. The bottle was stored inverted with water in the neck of the bottle.

Fracture orientations and densities were measured in the field in May 2003 and December 2003. Fracture density was measured using the circle-inventory approach of Davis and Reynolds (1996). Circles were created by using a 0.84-meter diameter hula-hoop. The total fracture length was determined by summing all the fracture lengths in the circle. Fracture density was determined by dividing the total fracture length by the radius

of the circle. The orientation and length for each fracture was then measured. The locations of fracture density circles were determined by surveying.

A photo mosaic was compiled of the southern canyon wall using Adobe Photoshop. On the mosaic, fractures were traced and measured for length, density, trend, and number of intersections. Densities were determined using a similar method as the one used in the field; circles of equal size were drawn side by side on the photo.

LABORATORY ANALYSIS

Solute Samples

Solute abundances were measured in the Department of Geology Hydrogeochemistry Laboratory at Brigham Young University in accordance with standard EPA methods (EPA, 1983). Anion analysis was performed on a Dionex ICS-90 Ion Chromatography System and a Mettler Toledo DL50 *Graphix* titrator. Cation and silica analysis were done using atomic absorption spectrometry on a PerkinElmer 5100 Atomic Absorption Spectrometer. The solute chemistry for each sample is reported in terms of mg/L and meq/L. The charge balance errors for these samples were all below 5%, with an average error balance of 2.95%. Saturation indices were calculated using the computer code WATEQF (Plummer et al., 1976). The gas sample was analyzed using Gas Chromotography (GS) at Skyline Coal mine, UT.

Isotope chemistry

Analysis for stable isotopes, $\delta^{2}H$ and $\delta^{18}O$ were performed at Brigham Young University (BYU) on a Finnigan Delta^{plus} mass spectrometer. One sample was analyzed for Tritium (^{3}H). Processing and analysis was done at BYU, similar to the method of the

University of Waterloo Environmental Isotope Laboratory (EIL, 1998). Tritium analysis was done on a PerkinElmer Quantualus 1220 Liquid Scintillation Counter (LSC). Typical values of uncertainty were ±1‰ for δ^2H and ±0.3‰ for $\delta^{18}O$.

GEOLOGIC SETTING

STRUCTURE

The Hurricane Fault is located in the transition zone of the Basin and Range and the Colorado Plateau physiographic provinces. To the west, the Basin and Range is characterized by thin crust (~30 km), east-west trending extensional tectonics, and extensive igneous activity. To the east, the Colorado Plateau is a relatively tectonically stable region with generally horizontal strata, that region has experienced broad regional uplift.

The Hurricane fault is exposed at the mouth of Timpoweap Canyon (Figure 3). The Hurricane fault extends 250 km from the Grand Canyon area in Arizona to north of Cedar City, Utah (Stewart et al., 1997). The Hurricane fault is listric with small antithetic horst and graben structures produced from reverse drag on the fault (Budding and Sommer, 1986). East of the Hurricane Fault, the strata are jointed and dip gently to the northeast (Biek et. al., 2000). West of the Hurricane Fault, the strata have been folded and fractured by the Virgin Anticline. The Virgin Anticline, Cretaceous to early Tertiary age, is northeast trending, generally symmetrical, and plunges to the north (Biek, 2000).

At Timpoweap Canyon, the fault displaces Paleozoic rocks in the footwall against Permian and Triassic rocks in the hanging wall (Figure 4). The first movement along the fault is estimated to be late Miocene to early Pliocene and the latest movement is

considered Holocene (Biek, 2003; Stewart et al., 1997). At Timpoweap Canyon, the strike of the Hurricane Fault is N10°E with a westward dip of 75° (Biek, 2003). Where the fault crosses the Virgin River, displacement occurs along a series of parallel segments to comprise a complex fault zone (Figure 4). The total displacement of the Hurricane Fault is estimated to be 2400 to 3000 m at Hurricane (Biek, 2003). The core zone is about 200 meters wide (Biek, 2003). The U.S. Bureau of Reclamation (1974) suggested the complex fault zone is a barrier to groundwater circulation. At the surface, the core of the eastern most fault consists of fine-grained Moenkopi Formation gouge. All spring and CO_2 gas discharge, in the Virgin River Canyon, occurs from the eastern damage zone located immediately east of the eastern most fault segment. At the surface the damage zone discharges occur from the Toroweap Formation along a 470-meter wide reach of the Virgin River (Figure 5).

STRATIGRAPHY AT TIMPOWEAP CANYON

The hanging wall of the Hurricane Fault consists of Cretaceous and older sedimentary rocks (Figure 4 and 6). The footwall, including the Timpoweap Canyon consists of Permian and older sedimentary rocks. The geology of Timpoweap Canyon is shown in Figure 3. The Queantoweap Sandstone is not exposed in the canyon, but underlies the Toroweap Formation (Figure 4 and 6). The Queantoweap is a massively bedded to cross-bedded, very fine to fine-grained, noncalcareous sandstone. The sandstone is highly fractured near the Hurricane fault zone. The strata are estimated to be 450 to 600 meters thick. The upper contact is an unconformity with the Seligman Member of the Toroweap (Biek, 1998).

The Toroweap Formation consists of the Seligman, Brady Canyon, and Woods Ranch Members, in ascending order (Figure 4). In the Hurricane Quadrangle, the Seligman Member is 9 to 15 meters thick and is composed of fine-grained sandstone and siltstone, which is locally gypsiferous. In the Timpoweap Canyon, the Brady Canyon Member is 60 meters thick and is thick-bedded limestone and cherty limestone. The Woods Ranch Member is 30 meters thick. It consists of interbedded dolostone, chert, gypsum mudstone, and limestone. Above the Toroweap Formation, the Kaibab Formation is about 90 meters thick in the canyon and consists of a limestone member, interbedded gypsiferous mudstone, and limestone. The Moenkopi Formation overlies the Kaibab Formation (Figure 4 and 6). Near the springs, the Moenkopi Formation is approximately 45 meters thick, consisting of interbedded conglomerate, limestone, mudstone, siltstone, fine-grained sandstone, and gypsum (Biek, 1998).

RESULTS

In the Timpoweap Canyon, the total measured gain of the Virgin River from spring discharge was about 260 L/s (Table 1, Figure 5). The term spring is used herein to describe all above and below river bedrock groundwater discharge. The overall downstream increase in spring discharge in the 470 m wide damage zone was relatively constant at about 0.63 L/sec/m. However, there were two locations (F2 to F3 and F9 to F12) where little increase in spring discharge was observed (Figure 7). The largest spring discharge occurred between locations F5 and F6. For atleast 450 meters downstream, no springs were found in the hanging wall of the fault (Figure 8).

Damage zone CO_2 gas discharges do not follow the pattern of spring discharge; instead, there are three areas in which the gas discharge significantly increases, one

occurring within 37 to 122 meters of the fault (Table 2, Figure 9). The area with the largest number of gas vents occurs approximately 259 to 335 meters from the fault, this area coincides with the largest spring discharge (Figure 7 and Figure 9). The other area of significant gas discharge occurs from 365 to 444 meters from the fault. The areas of significant gas flow are labeled two, four and six on Figure 9. Areas of low gas flow are labeled one, three, five, and seven. In thirteen intervals there were no vents (Table 2). Many intervals of zero gas discharge correlate with areas of little increase in spring flow. CO_2 gas also does not discharge west of the fault.

The total gas outflow volume was measured in the areas of significant gas discharge (Table 3). To estimate the total volume of gas discharge for the areas two, four, five, and six, the measurements located in each area were added (Figure 9). Estimations were made for the volume of gas for areas one, three and seven (Table 3). The total estimated gas discharge for Timpoweap Canyon is about 4.9 L/s. Group two has the largest discharge of 2.2 L/s.

Water samples were collected from the Virgin River, upstream and downstream of the springs, and from several of the large springs (Figure 10). The spring waters are thermal, with an average temperature of 40.2˚C (Table 4). The waters have a pH averaging 6.3. The solute compositions of the springs are similar; sodium-chloride type with elevated total dissolved solids (TDS) averaging 8491 mg/L (Figure 11). The Virgin River upstream of the springs is a mixed cation-bicarbonate type with a mean TDS of 414 mg/L, whereas the Virgin River downstream samples are sodium-chloride type with a mean TDS of 7674 mg/L (Table 4). The increased temperature and TDS and decreased pH in the downstream Virgin River samples exhibit mixing of Virgin River water with

spring water. Flow of the Virgin River can vary from 15 to 3000 L/s because of storm events and releases from the Quail Creek Diversion Dam (U.S. Bureau of Reclamation, 1974). At the time of sampling, the flow of the Virgin River below the diversion dam was only 16 L/s. Thus, the chemistry of the Virgin River downstream of the springs varies depending on the amount of flow that is diverted upstream.

The solute composition for the springs is consistent with previous studies (Cordova, 1981; Budding and Sommer, 1986; and Mundorff, 1970). The chemistry has not significantly changed over the last sixty years, except in 1985-1987. In 1985, the Pah Tempe spring discharge almost doubled, temperature decreased by 5ºC, and specific conductivity decreased by 15%. This dramatic change resulted from sinkholes that had developed in the Kaibab Formation in the bed of the Virgin River near the Quail Creek diversion, approximately 3.2 km upstream from the springs (Everitt and Einert, 1994). About 850 to 1130 L/s of the Virgin River discharged into the sinkholes, and the spring discharge doubled soon after. The dilution and increased discharge of the springs was a result of mixing with the Virgin River. After the Virgin River was diverted around the sinkholes, the springs began to recover within a year and returned to normal after two and a half years (Everitt and Einert, 1994).

Table 5 shows the saturation indices for the spring water, indicating they are supersaturated with respect to quartz, calcite, aragonite, and dolomite, and undersaturated with respect to gypsum and halite. Carbonate precipitation occurs as result of CO_2 degassing of the carbonate mineral waters to supersaturation when the waters reach the surface. Small amounts of tufa deposits have formed at the larger springs, and older tufa deposits occur as ledges and pockets high on the south canyon wall. The rate of tufa

precipitation is slow. Downstream of the spring discharge, the Virgin River waters are supersaturated with respect to calcite, aragonite, and dolomite, and undersaturated with respect to gypsum and halite at low flow conditions. Tufa deposits are not present in the bed of the Virgin River, which is likely due to the nature of the sandy bed and the velocity of the river.

ISOTOPES

The δ^2H and $\delta^{18}O$ values were plotted relative to the global mean meteoric water line (GMWL, Figure 12). The upstream Virgin River lies along the GMWL; however the springs plot to the right of the meteoric water line. The Pah Tempe spring waters are more depleted in δ^2H than upstream Virgin River (Table 5, Figure 12). The downstream Virgin River stable isotope composition exhibits mixing of upstream Virgin River and spring water.

The $\delta^{13}C$ value for the gas vent sample was -5.3 ‰. At a pH of 6.3, the HCO_3^- and H_2CO_3 are almost equal so a weighted $\delta^{13}C$ must be calculated by the abudance of each species. A $\delta^{13}C$ value for the HCO_3^- of the spring water was calculated from the gas, using the following equations (Mook et al., 1974 and Friedman and O'Neil, 1977):

$$1000 \ln \alpha = E \frac{10^3}{T} + F \qquad (1)$$

where $1000 \ln \alpha = 6.38$ at 40.2ºC. (2)

and

$$1000 \ln \alpha = \delta_{HCO_3} - \delta_{CO_2(g)} \qquad (3)$$

Using equation 3, with 6.38 for 1000 * ln α and -5.3‰ for the CO_2 (g) $\delta^{13}C$, and solving for δ_{HCO3} results in a $\delta^{13}C$ of 1.1 ‰ for the spring water. A $\delta^{13}C$ value for the $H_2CO_3^-$ of the spring water was calculated from the gas, using the following equations (Mook et al., 1974 and Friedman and O'Neil, 1977):

$$1000 \ln \alpha = D\frac{10^6}{T^2} + E\frac{10^3}{T} + F \qquad (4)$$

where $1000 \ln \alpha = -0.84$ at 40.2ºC. (5)

and

$$1000 \ln \alpha = \delta_{H_2CO_3} - \delta_{CO_2(g)} \qquad (6)$$

Using equation 6, with -0.84 for 1000 * ln α and -5.3‰ for the CO_2 (g) $\delta^{13}C$, and solving for δ_{H2CO3} results in a $\delta^{13}C$ of -6.14 ‰ for the spring water. The molality calculated in WATEQ (Plummer et al., 1976) was used to find the abundance of each species in the water. The calculated weighted $\delta^{13}C$ CO_2 (g) for the spring water is -1.9.

Tritium was <0.2 TU (tritium units; table 5), which signifies that the springs are submodern or older (pre-1952; Clark and Fritz, 1997). It was not possible to determine a ^{14}C age because of the excess dead carbon in the system (Mayo, 2004).

FRACTURES

Fractures in Timpoweap Canyon have a general strike of north to N30°E, subparallel to the Hurricane Fault (Figure 13). Sixty percent of the fractures were ≤1 mm in width, thirty-five percent were 2 to 5 mm in width, and five percent were greater than 9 mm in width. The average fracture density is 4.08 m/m^2 with a standard deviation of 1.85 m/m^2 (Table 6). The maximum of 9.44 m/m^2 occurred at FR38 and a minimum of 0

m/m^2 occurred at FR2 and FR3 (Figure 13, Table 6). The areas of high fracture densities occur at 230 and 280 meters east of the fault (Figure 13). High fracture density refers to areas where the density exceeds the mean and the highest fracture density exceeds the mean by at least one standard deviation (5.9 m/m^2). Low fracture density refers to areas which have density less than one standard deviation from the mean (2.23 m/m^2). Areas of low density occurred west of the fault and 110 and 300 meters east of the fault.

The fracture traces from the photo mosaic are shown in Figure 14. The average density was 1.21 cm/cm^2 with a standard deviation of 0.51 cm/cm^2 (Table 7). The maximum of 2.45 cm/cm^2 occurred at CR55 and a minimum of 0.06 cm/cm^2 occurred at CR38. Areas of high fracture densities (>1.21 m/m^2) occur at 180 and 310 meters west of the fault (Figure 13). Areas of highest fracture densities are greater than one standard deviation from the mean (1.7 m/m^2). Areas of low density (<0.70 m/m^2) occurred at 350 meters from the fault. The areas of high fracture density from the photo mosaic correlate fairly well with the areas of fracture density from the field

To compare fracture density to spring and gas discharge, the canyon was divided into areas, which are discussed further below (Figure 15). These areas were chosen based on the areas of gas discharge and are discussed beginning near the fault and continuing upstream (Figure 9).

Area one is located by the eastern edge of the core zone of the Hurricane Fault (Figure 15). West of the fault there are no springs or gas discharge and the fracture density is below the average. The low density is because the clay-rich Moenkopi Formation deformed in a more ductile manner so it does not sustain fractures. The area between the fault and area two has low gas discharge. The volume of CO_2 gas is

estimated at 0.06 L/s which is less than one percent of the total gas discharge in the canyon. There are no data on fracture density in this area because the area is smaller than the distance between most field density measurements and vegetation cover on the photo mosiac.

Area two is the closest large gas discharge to the fault. The area is characterized mostly by high fracture density yet the eastern end has low density. There are two large springs (approximately 20 to 40 L/s of discharge) and several smaller springs. The western edge of the area has low spring discharge (Figure 15).

Area three has low gas discharge (0.24 L/s). There are many small springs (0.1 to 2 L/s) but no larger springs. The area has high fracture density on the eastern end and low density on the west end where there are no gas vents (Figure 15).

Area four is characterized by the highest spring and gas discharge (Figure 5, 9). The volume of gas discharges in this area is almost fifty percent of the total gas discharge of the canyon. There are many springs both large and small that discharge in the area. Two springs discharge an estimated 30 L/s combined. The area has mostly high fracture density with only a few locations of low density (Figure 15).

Area five is characterized by mostly low fracture density and low gas discharge (0.2 L/s). Only a few small springs discharge in this area.

Area six is the last area of high gas discharge (about 1.0 L/s). The area has high fracture density on east end but had areas of low density in the west end. It has low spring discharge, yet there are three springs that discharge 2 to 7 L/s and one spring with an estimated discharge of 20 L/s.

Area seven has low gas discharge. There are several small springs and one large spring. The large spring discharges from a pipe located on the north bank of the river. In summary, areas two, four and six have the high spring and gas discharge with generally high fracture density. Areas one, three, five, and seven have low spring and gas discharge with generally low fracture density.

DISCUSSION

DEPTH OF CIRCULATION

The potential depth of groundwater circulation was evaluated using groundwater discharge temperature, silica geothermometers and other estimates. Alkaline geochemical thermometers were not used because of the excessive Na^+ in the groundwater. Budding and Sommer (1986) reported a geothermal gradient of 18.5º to 33.7ºC/km. The mean annual air temperature of is 16.1˚C (U.S. Bureau of Reclamation, 1974).

The average discharge temperature of the springs is 40.2˚C. The difference in temperature of the springs and mean annual temperature is 24.1˚C. Potential depths of circulations are calculated by dividing the difference in temperature by the geothermal gradient (Table 8). An uncertainty of 1˚C in the mean annual temperature results in an uncertainty of ~30 m in depth. Two end member solutions were calculated using the geothermal gradient report by Budding and Sommer (1986), giving circulation depths ranging from 0.72 km to 1.3 km (Table 8). The formations at this depth are likely to be the Pakoon Dolomite, Callville Limestone, and Redwall Limestone (Figure 4 and 6). This approach gives a minimum circulation depth because it does not consider any cooling during the ascent of the groundwater. Mixing with cooler shallower groundwater

would also increase the uncertainty of circulation depth. The minimum depth that the groundwater must be circulating is the Pakoon Dolomite.

Geothermometers can be used to calculate the maximum subsurface temperatures. Geothermometers rely on the assumptions that the chemical reactions are temperature dependent, that chemical equilibrium exists between the water and the specific minerals which supply the chemical constituents, and that the chemical composition of the water does not change as it ascends from the aquifer to the surface (Clark and Fritz, 1997). For the Pah Tempe springs, Budding and Sommer (1986) calculated an average reservoir temperature of 80˚C using a quartz geothermometer and Na-K-Ca-Mg geothermometer. Aquifer temperatures were calculated using chemistry from spring samples 9, 10, and 11 and are shown in Table 9. The calculated chalcedony, cristobalite, and amorphous silica geothermometer temperatures are underestimations since they are lower than the measured surface temperature of the water. This may be a a result of water-rock re-equilibration. The reservoir temperature range is 70-75ºC based on conductive and adiabatic silica geothermometers, which is less than the temperature Budding and Sommer (1986) calculated. Based on this range, the circulation depth would be between 1.6 km and 3.2 km (Table 8). At this depth the rock formations are the Nopah Dolomite, Muav Limestone, Bright Angel Shale, Tapeats Sandstone, and basement bedrock. A more accurate depth of circulation could be calculated with accurate formation thicknesses and a smaller, more accurate range for the geothermal gradient. The geothermometers indicate a minimum subsurface temperature and minimum circulation depth.

The stable isotopes, δ^2H and $\delta^{18}O$, of the spring waters plot to the right of the meteoric water line in a positive trend with a slope of zero, indicating a water-rock exchange of oxygen isotopes (Figure 12). High temperature geothermal water (>100ºC) may equilibrate with oxygen in clays and other aluminosilicate minerals, which causes a positive shift from the GMWL (Clark and Fritz, 1997). It is likely that the spring waters have experienced temperatures >100ºC. Circulation depths were calculated for aquifer temperatures of 100°C and 125°C, placing circulation depths in the basement bedrock (Table 8).

Based on chemical geothermometers, the maximum subsurface temperature is range is about 70°C to 75°C; the minimum reservoir depth is the Nopah Dolomite and maximum reservoir depth the basement bedrock. However, the stable isotopes show that the spring water has exceeded 100°C. This means the water has cooled and silica re-equilibrium has occurred invalidating the silica geothermometers and the more likely reservoir is the basement bedrock.

RECHARGE AREA

The local annual precipitation is about 31 cm, yet the estimated infiltration rate is only 3 cm per year (NCDC, 2005; Cordova, 1981). The recharge area needed to supply the Pah Tempe springs would be 275 km^2. Groundwater infiltrates, possible flowing first westward until it reaches the Hurricane Fault. Then it travels along the damage zone in a formation at least as deep as the Pakoon Dolomite and more likely as deep as the basement bedrock. The basement bedrock may be highly fractured at depth from Hurricane faulting, however with increasing depth the density and aperture of fractures

decreases due to increased lithostatic pressure. The fracturing of the basement bedrock is a good reservoir for groundwater.

The Virgin River follows a regional orthogonal fracture set (Figure 16). This fracture pattern was not measured in the canyon yet the pattern of the stream suggests a fracture system perpendicular to the Hurricane Fault. The Pah Tempe springs are an area were this pattern intersects the Hurricane Fault. This East-West fracture pattern allows a route to the surface for the deep water at the canyon.

The elevated Cl^- and Na^+ concentrations (about 100 meq/L) suggest halite dissolution although the waters are halite undersaturated (Table 4). The average Cl^-/Na^+ ratio is 0.93 which means that the Cl^- and Na^+ is dissolved from halite, however, Na^+ is in excess in three samples and Cl^- is in excess in two samples (Table 4). The elevated SO_4^{2-} concentrations (37 meq/L) relative to upstream water suggest gypsum dissolution (Table 4). The H_2S odor in the canyon suggests some sulfate reduction. The ionic ratios of HCO_3^-/Ca^{2+} are about 0.57, which, if only carbonate dissolution were occurring in the system, the ratio should be one. Excess Ca^{2+} is entering the system by gypsum dissolution, ionic exchange, or HCO_3^- may have been removed from the system from CO_2 degassing, or both. The elevated SO_4^{2-} suggests that gypsum dissolution is occurring and can account for all of the excess Ca^{2+}. The large volume of CO_2 gas at the surface would also suggest that degassing is occurring.

From calculations based on the concentrations of Na^+ and discharge rate of the springs, the estimated volume of halite that is dissolved a year is 2.22×10^4 m^3. Groundwater from the Upper Virgin River Basin in the Chinle Formation have concentrations of Na^+ of 18 meq/L and a well into the Moenkopi Formation in the Kanab

Creek Basin had concentrations of 109 meq/L (Cordova, 1981). Other groundwater samples from this formation had levels much lower. There is a possibility of obtaining high sodium and chloride concentration from the Moenkopi Formation. This is supported on the type of sediment in the Moenkopi and on the elevated concentrations found in the Moenkopi well.

Several formations may have gypsum and could be a source of the SO_4^{2-} concentrations. From calculations based on the concentration of the SO_4^{2-} and the discharge of the springs, the estimated volume of gypsum that is dissolved a year is 8.83 x 10^3 m^3. The Moenkopi Formation and Seligman Member of the Toroweap Formation are possible sources of the gypsum.

Water samples 10 and 11 were taken from springs directly north and south of the river to determine if the isotopes were the same on each side (Table 5, Figure 10). They have similar isotope values indicating that the springs on both sides of the river have the same source. The δ^2H isotopic composition of the spring water samples are more negative than the Virgin River samples, which suggests a colder climate or higher elevation of recharge than the Virgin River (Table 5, Figure 12). The headwaters of the Virgin River recharge at an elevation around 3000 meters. Much of the water of the Virgin River comes at elevations around 2400 meters. The spring water may recharge at higher elevations. More likely the spring water recharged during a colder climate.

CARBON HISTORY

Processes that may generate the CO_2 gas include: 1) the degradation of organic matter; 2) gases derived from mantle or magmatic sources; 3) diagenetic reactions

involving clay and carbonate rocks; and 4) thermal decarbonation of carbonate rocks by metamorphic processes (Cappa and Rice, 1995, and Mayo and Muller, 1997).

The degradation of organic matter from hydrocarbons produces CO_2 $\delta^{13}C$ values of -8 to -12‰ (Hunt, 1996). The CO_2 gas value in the Timpoweap Canyon is not in this range. The degradation of organic matter through sulfate reducing bacteria could occur when SO_4^{2-} concentrations are >1.1 meq/L and temperatures less than 80ºC (Carothers and Kharaka, 1980). The expected range of $\delta^{13}C_{HCO3-}$ of <-10‰ is more depleted than the value $\delta^{13}C_{HCO3-}$ calculated for the springs. Also results from the isotopes show that the temperatures exceed 80ºC, the temperature needed for the reaction for sulfate reducing bacteria. Methanogenic bacteria can also degrade organic matter, yet they do not thrive in waters with SO_4^{2-} concentrations above 1.1 meq/L (Carothers and Kharaka, 1980). The spring water has concentrations around 78 meq/L, which are significantly higher than 25 mg/L.

The stable isotopes, δ^2H and $\delta^{18}O$, of the spring water are beyond the range for magmatic water, so any contribution of magmatic water is minimal. However, the $\delta^{13}C$ of the CO_2 gas is within the range of magmatic and mantle CO_2. Magmatic degassing could be responsible for generating the gases in the area. Evidence for recent basaltic volcanism is seen throughout the Hurricane Quadrangle (Biek, 2003). Values typical of CO_2 from a degassing mantle or igneous melt source range from 0 to -4‰ (Siegel et al., 2004). Clark and Fritz (1997) report a range of -3 to -10‰ for mantle CO_2. The CO_2 gas could be traveling through fractures and pore space of the bedrock, yet because of lithostatic pressure the permeability of the rock would be small. Mantle degassing is not a likely source since it would be difficult for the gas to travel from the mantle, yet the

$\delta^{13}C$ of the Pah Tempe gas is well within the range of mantle gas and may be a possible source. The other processes listed are discussed below as possible additional sources of the $\delta^{13}C$ value.

Diagenetic reactions involving clay and carbonate rocks occur at temperatures between 100ºC and 200ºC (Hunt, 1996; Mayo and Muller, 1997). Using the geothermal gradient, possible stratigraphic formations that would reach temperature of at least 100˚C are buried 2.5 km to 4.5 km. However, this is below the Tapeats Sandstone. The formation below the sandstone is the basement bedrock. The basement bedrock was metamorphosed in the Precambrain and so would not be a likely source for the CO_2 gas. Diagenetic reactions could occur in the Bright Angel shale or the Muav Limestone if temperatures were high enough. If the formation depths of the stratigraphic column are underestimated or if the geothermal gradient is higher because of nearby volcanic activity, then the Bright Angel Shale and the Muav Limestone could possibly be sources of the CO_2 gas through diagenesis.

Thermal decarbonation of carbonate rocks by metamorphic processes would occur at high temperatures (450°C; Mayo and Muller, 1997). However, high temperatures are unlikely based on burial depth of the carbonate formations. Yet contact metamorphism may have occurred because the nearby basaltic activity. The most recent basalt flows at 0.14 Ma years old and another recent flow at 0.258 Ma years ago. These igneous intrusions could cause metamorphism of the lower rock formations and be a possible source of CO_2 gas. The batholith which sourced the basalt flows would likely have cooled and crystallized and the CO_2 gas would have dissipated sometime in the past.

If the rocks were metamorphosed, then the temperature gradient would be higher, so the depth of circulation would be less.

CO_2 gas probably traveled up through fractures along the fault and mixed with the water at a higher elevation. The processes that may have generated the CO_2 were from a mantle, magmatic source, or diagenesis of clay or carbonate rocks. Thermal decarbonation by metamorphic processes and the degradation of organic matter have not contributed any CO_2. Further research into the stratigraphic formations below the Queantoweap Sandstone, ^3He / ^4He data, and the geothermal gradient may help to clarify the source of the CO_2 gas.

FRACTURES

The density of the fractures observed at the macroscale (outcrop) and mesoscale (photo mosaic) are slightly discordant. In some areas each scale of observation have opposite trends. These differences may occur impart due to poor exposure of canyon wall because of vegetation. Error also might have occurred because of the difficulty in matching the location of the photo mosaics circles with the survey information.

Peacock (2001) indicated that the damage zone of a fault in an ideal situation would have the highest density near the fault and decrease away from it. He noticed that an increase in fracture density toward the fault indicated the fractures formed synchronous with fault development. Other variations in fracture patterns or frequency indicate pre- or post-faulting fractures. In Timpoweap Canyon, the fracture density does not decrease from the fault (Figure 17). The data collected for the canyon is only showing a portion of the damage zone nearest to the fault. More analysis farther from the fault would be needed to fully define the damage zone. The fracture density pattern is

most likely influenced by pre-faulting fracture sets perhaps associated with subsidiary faults, collapse from gypsum dissolution, and Sevier Orogeny deformation. Subsidiary faults found east of the main Hurricane Fault may have caused more fracturing in the immediate area to the faults. Two areas in particular show evidence of increased fracture density associated with pre-existing faults. They are approximately 225 and 420 meters from the fault in gas discharge areas six and four (Figure 15 and 17). These areas are likely associated with the fracture system that the Virgin River follows. Fracturing may have occurred as a result from the collapse structures from gypsum dissolution in the Seligmen Member. Also the fractures could be pre-faulting fractures.

As the water travels through the Seligmen Member it dissolves gypsum. The gypsum dissolution causes collapse structures. The areas which collapse closes the voids space and decreases permeability. The edge of these collapse structures create the subsidiary faults or large bedding plane crossing fractures which may allow larger spring discharging such as area four.

FRACTURE FLOW

Budding and Sommer (1986) found the Toroweap Limestone in the Timpoweap Canyon has near-surface cavernous permeability, which facilitates the high discharge of the Pah Tempe springs. The water pressure is from the pressure head in the recharge area. As discussed previously, Everitt and Einert (1994) studied the surge in the discharge of the Pah Tempe Springs in 1985. This supports the theory of near-surface cavernous porosity and high discharge of Toroweap Formation. Everitt and Einert (1994) proposed a conceptual model for the source of water in the Pah Tempe Springs; the model shows deeply circulated groundwater rising and mixing with water from the Virgin

River in the Queantoweap Formation. However, there is minimal mixing with Virgin River water because the tritium concentrations in the springs are <0.2 TU. This could be a result of low amounts of water allowed past the diversion dam through the canyon during sampling.

The spring discharge does not follow the expected pattern of decreasing discharge with increasing distance from the fault; instead it has a nearly linear pattern (Figure 18). The expected pattern of discharge is based on the hypothetical decreasing density pattern of a typical fault. As density decreases away from the fault spring discharge would be expected to decrease also. Since the fracture density in the canyon does not follow the expected pattern, neither do the springs. Yet the spring discharge does not completely mimic the fracture pattern. Between gas discharge areas one and two, there is a relative high fracture density with low spring and gas discharge (Figure 15). The eastern end of area one has low fracture density and parts of area three and two have areas of low fracture density.

The areas of highest gas and spring discharge correlate with intersections of the orthogonal fracture set with the fractures from the Hurricane Fault. These areas occur about 220 meters from the fault (area four) and 400 meters from the fault at the bend in the river (area six, Figure 15). Many areas of spring discharge are associated with large inter-bedding fractures and subsidiary faults. The highest spring and gas discharge, in area four, occur just east of a fault (Figure 15). This fault is an intersection of the orthogonal fracture set and fractures from the Hurricane fault. This fault may be acting as a conduit of flow for area four. Some of the larger springs and increases in gas

discharge in area six are closely associated with large fractures. These large fractures are likely part of the orthogonal fracture set that the Virgin River follows.

Flow may be affected by gypsum dissolution in the Seligman Member. The Seligman Member is just below the riverbed of the Virgin River in the canyon (Figure 4). The formation contains significant amounts of gypsum that is likely to be dissolved leaving caverns or voids, causing the overlying rocks to collapse. The collapsed areas would decrease pore space and as a result decrease permeability in these areas. Area one and three are possible areas that may have lower permeability from gypsum dissolution. The two large springs in area two are also associated with faults that may be from collapse blocks from gypsum dissolution.

CONCLUSION

The Pah Temp spring water was circulated to a depth at least 0.72 km below the ground surface and may have been circulated as deep as 5 km. The positive geothermal shift of the stable isotopes denotes that the groundwater temperature has exceeded 100°C. Based on circulation depths calculated from temperatures greater than 100°C, the most likely reservoir would be the basement bedrock. Groundwater temperature could have been heated by other sources and not just deep circulation.

The recharge needed to supply groundwater for the Pah Tempe springs is large (275 km^2). Stable isotopes suggest that the recharge for Pah Tempe springs is from a colder climate than the Virgin River water. Groundwater may travel west toward the Hurricane Fault, then parallel to the fault to the springs. The model proposed by Everitt and Einert (1994) does not occur during low flow conditions of the Virgin River as shown by the tritium values.

The CO_2 gas might be generated from a mantle source or diagenetic reactions involving clay and carbonate rocks. The CO_2 likely traveled from the source of generation up the fault along fractures, then mixed with the spring waters.

The fracture density and spring discharge in the Timpoweap Canyon do not decrease with increasing distance from the Hurricane Fault as is expected. As suggested by Peacock (2000) only fractures that form synchronously with the faulting will tend to decrease in frequency away from the fault. The fractures of the Hurricane Fault damage zone do not display a decreasing tendency away from the fault as a result of pre-faulting stresses from the Laramide and Sevier Orogenies. The fracture analysis has shown that intersection of pre-faulting fractures with fractures formed from the Hurricane fault, subsidiary faults, large continuous fractures, and gypsum dissolution have affected the location of spring discharge.

REFERENCES

Beus, S. S., 1987, Geology along the South Kaibab Trail, eastern Grand Canyon, Arizona. In: Geological Society of America Centennial Field Guide – Rocky Mountain Section, 1987 pp. 371-378

Biek, R., 2003, Geologic map of the Hurricane Quadrangle Washington County, Utah: Utah Geological Survey 187, scale 1:24,000.

Biek, R. F., 2000, Geology of Quail Creek State Park, Utah. In: Geology of Utah's Parks and Monuments, Eds. Sprinkel, D. A., Chidsey, T. C., and Anderson, P. B. pp. 465-477.

Biek, R. F., Willis, G. C., Hylland, M. D., and Doelling, H. H., 2000, Geology of Zion National Park, Utah. In: Geology of Utah's Parks and Monuments, Eds. Sprinkel, D. A., Chidsey, T. C., and Anderson, P. B. pp. 107-135.

Budding, K. E. and Sommer S. N., 1986, Low-Temperature Geothermal Assessment of the Santa Clara and Virgin River Valleys, Washington County, Utah. *Utah Geological and Mineral Survey*, v. 67, 34 p.

Caine, S. C.; Evans, J. P.; and Forester, C. B., 1996, Fault zone architecture and permeability structure: *Geology*, v. 24, no. 11, p. 1025-1028.

Carothers, W. W., and Kharaka, Y. K., 1980, Stable carbon isotopes of HCO_3^- in oil-field waters - implications for the origin of CO_2. *Geochimica et Cosmocimica Acta,* v. 44, p. 323-332.

Clark, I. D., and Fritz, P., 1997, Environmental Isotopes in Hydrogeology, Boca Raton: CRC Press, Lewis Publishers.

Cordova, R., 1981, Ground-water Conditions in the Upper Virgin River and Kanab Creek Basins Area, Utah, with Emphasis on the Navajo Sandstone. Utah Department of Natural Resources, Division of Water Rights, no. 70, 87 p.

Davis, G. and Reynolds, S., 1996, Structural Geology of Rocks and Regions, John Wiley, 776 p.

Environmental Isotopes Laboratory, 1998, Tritium Analysis: Technical Procedure 1.0, Department of Earth Sciences, University of Waterloo.

EPA, 1983, Methods for chemical analysis of water and wastes-EPA-600 4-79-020: National Exposure Research Laboratory, Cincinnati, Ohio.

Everitt, B. and Einert, M., 1994, The 1985 Slug Test of Pah Tempe Springs Washington County, Utah. Utah Geological Association Publication, v. 23, p 189-194.

Evans, J. P., Forster, C. B., and Goddard, J. V., 1997, Permeability of fault-related rocks, and implication for hydraulic structure of fault zones. *Journal of Structural Geology*, v. 19, issue 11, p. 1393-1404.

Friedman, I. and O'Neil, J.R., 1977, Compilation of stable isotope fractionation factors of geochemical interest, U.S. Geological Survey Professional Paper, 440-KK, 49 p.

Gudmundsson, A., 2001, Fluid overpressure and flow in fault zones: field measurements and models: *Tectonophysics*, v. 336, p. 183-197.

Harris, R.; Luthi, A.; Mayo, A. L.; and Koontz, W., 2002, Structural Controls of hydrodynamic anisotropy in the West Elk Mine Region, Western Colorado: *Environmental and Engineering Geoscience*, v. 8, n. 4, p. 309-318.

Harris, J. E., 1993, Anderson Junction. In: Oil and Gas fields of Utah, Utah Geological Association Publication, No. 22, 198 p.

Hintze, L. F., 1988, Geologic History of Utah, Brigham Young University Special Publication, No. 7.

Mayo, A. and Muller, A. B., 1997, Low temperature diagenetic - metamorphic and magmatic contributions of external CO_2 gas to a shallow ground water system. *Journal of Hydrology,* v. 194, p. 286-304.

Mayo, A., 2004, Department of Geology, Brigham Young University, personal communication.

Mook, W.G., Bommerson, J.C., and Staverman, W.H., 1974, Carbon isotope fractionation between dissolved bicarbonate and gaseous carbon dioxide, Earth and Planetary Science Letters 22, p. 169-176.

Mundorff, J. C., 1970, Major Thermal Springs of Utah. Water Resources Bulletin Salt Lake City, v. 13, 60 p.

NCDC, 2005, National Climatic Data Center, National Environmental Satellite, Data, and Information Service, Accessible at http://www.ncdc.noaa.gov/oa/ncdc.html

Plummer, L. N., Jones, B. F., and Truesdell, A. H., 1976, WATEQF – a FORTRAN IV version of WATEQF, a computer program fro calculating chemical equilibrium of natural waters. US Geological Survey Water Resource Investigation, 76-13, p 61.

Rawling, G. C.; Goodwin, L. B.; and Wilson, J. L., 2001, Internal architecture, permeability structure, and hydrologic significance of contrasting fault-zone types: *Geology*, v. 29, no. 1, p. 43-46.

Siegel, D. I., Lesniak, K. A., and Frape, S., 2004, Isotopic geochemistry of the Saratoga Springs: Implications for the origin of solutes and source of carbon dioxide. *Geological Society of America*, v. 32, no. 3, p. 257-260.

Stewart, M.E.; Taylor, W. J.; Pearthree, P.A.; Solomon, B. J.; and Hurlow, H. A., 1997, Neotectonics, fault segmentation, and seismic hazards along the Hurricane fault in Utah and Arizona: An overview of environmental factor in an actively extending region in Mesozoic to Recent Geology of Utah: Geological Society of America Field Trip Guide Book, 1997 Annual Meeting, Salt Lake City, Utah: Brigham Young University Geology Studies, v. 42, pt. 2, p. 235-254.

Taylor, W. J.; Stewart, M. R.; and Orndorff, R. L., 2001, Fault segmentation and linkage: Examples from the Hurricane fault, Southwestern U.S.A.: *Utah Geological Association Publication 30*, p. 113-126.

U.S. Bureau of Reclamation, 1974, Colorado River water Quality Improvement Program, Point Source Diversion, La Verkin Spring Unit, Utah: Feasibility Report.

TABLES

Table 1: Composite Gain-Loss measurements of the Virgin River in Timpoweap Canyon. Locations are meters from the temporary bench mark (N4118002.47, E298647.54 UTM).

Station ID	Date	Location N (m)	Location E (m)	Elevation (m)	Distance from the fault (meters)	Cumulative Spring Discharge (L/s)	
F1	22-May-03	460.9	431.1	30.8	580	0.0	Protolith
F2	31-Mar-03	317.4	429.8	29.2	430	57.1	
F3	31-Mar-03	286.7	376.8	29.2	365	62.5	
F4	22-May-03	300.8	334.9	28.3	324	98.1	
F5	31-Mar-03	318.6	293.1	28.4	279	116.6	
F6	31-Mar-03	327.0	262.9	28.3	247	160.2	Damage
F7	13-May-03	333.1	246.7	28.2	230	166.4	zone
F8	13-May-03	339.8	211.1	27.9	195	171.9	
F9	13-May-03	401.8	95.1	26.5	63	247.8	
F10	13-May-03	413.9	64.9	26.8	30	248.4	
F11	31-Mar-03	421.3	56.2	26.7	20	249.7	
F12	13-May-03	439.7	15.6	26.1	-27	256.9	Core zone
Total Spring discharge				**256.9**	**L/s**		

Table 2: Gas vent counts in 6.1 meter intervals along Timpoweap Canyon. Intervals begin at the eastern most mapped trace of the Hurricane Fault. Locations are shown in Figure 7 and are in meters from the temporary bench mark (N4118002.47, E298647.54 UTM).

Interval (m)		Interval Length	Number of gas	Vents	Location		Interval (m)		Interval Length	Number of gas	Vents	Location	
Start	End	(m)	vents	per m	E	N	Start	End	(m)	vents	per m	E	N
0	6	6.1	0	0.0	37.4	432.8	274	280	6.1	69	11.2	285.3	319.3
6	12	6.1	20	3.3	42.7	429.6	280	286	6.1	67	10.9	291.0	317.2
12	18	6.1	8	1.3	48.1	427.1	286	293	6.1	230	37.4	297.1	315.0
18	24	6.1	5	0.8	53.9	424.2	292	299	6.1	130	21.2	302.9	313.0
24	30	6.1	6	1.0	59.5	422.1	299	305	6.1	145	23.6	308.6	310.8
30	37	6.1	30	4.9	64.8	419.4	305	311	6.1	145	23.6	314.4	309.1
37	43	6.1	64	10.5	70.2	416.8	311	317	6.1	4	0.7	320.1	307.2
43	49	6.1	21	3.4	75.8	414.1	317	323	6.1	47	7.6	325.7	305.1
49	55	6.1	25	4.1	81.3	411.6	323	329	6.1	20	3.3	331.1	302.7
55	61	6.1	30	4.9	86.8	408.9	329	335	6.1	40	6.5	336.4	300.3
61	67	6.1	12	2.0	91.9	406.6	335	341	6.1	38	6.2	342.6	298.0
67	73	6.1	83	13.6	97.6	403.9	341	344	3.0	0	0.0	348.6	296.0
73	79	6.1	2	0.3	103.0	401.3	344	350	6.1	0	0.0	351.6	295.9
79	85	6.1	24	3.9	108.5	398.6	350	356	6.1	7	1.1	357.9	296.0
85	91	6.1	65	10.7	114.1	396.0	356	362	6.1	32	5.2	364.0	296.0
91	98	6.1	50	8.2	119.2	393.6	362	365	3.0	5	1.7	370.3	296.4
98	104	6.1	58	9.5	124.7	390.5	365	371	6.1	30	4.9	373.3	296.6
104	110	6.1	0	0.0	129.6	387.1	371	377	6.1	94	15.4	379.2	296.7
110	116	6.1	0	0.0	134.7	383.5	377	383	6.1	60	9.8	385.1	297.7
116	122	6.1	10	1.6	139.7	380.0	383	389	6.1	10	1.6	391.2	298.3
122	128	6.1	43	7.0	144.6	376.6	389	395	6.1	17	2.8	397.8	298.7
128	134	6.1	20	3.3	149.7	373.2	395	402	6.1	30	4.9	404.2	299.2
134	140	6.1	0	0.0	155.0	370.7	402	408	6.1	18	3.0	410.1	299.8
140	146	6.1	0	0.0	160.5	367.6	408	414	6.1	6	1.0	415.2	302.3
146	158	12.2	0	0.0	166.2	364.6	414	417	3.0	7	2.3	420.8	305.1
158	164	6.1	1	0.2	176.9	359.0	417	420	3.0	10	3.3	423.7	306.6
164	170	6.1	0	0.0	182.5	356.5	420	426	6.1	12	2.0	426.1	308.9
170	176	6.1	0	0.0	187.5	353.9	426	432	6.1	21	3.4	429.7	313.8
176	182	6.1	0	0.0	192.5	350.9	432	438	6.1	22	3.6	432.6	318.9
182	188	6.1	13	2.1	198.1	348.6	438	444	6.1	67	11.0	435.4	324.3
188	195	6.1	13	2.1	204.3	346.3	444	450	6.1	44	7.2	437.5	330.2
195	201	6.1	26	4.3	210.2	344.7	450	457	6.1	7	1.1	440.3	335.7
201	207	6.1	7	1.1	216.2	343.3	457	463	6.1	1	0.2	443.1	341.1
207	213	6.1	21	3.4	222.2	341.7	463	469	6.1	20	3.3	446.7	346.4
213	219	6.1	2	0.3	228.0	340.2	469	475	6.1	3	0.5	448.5	350.6
219	225	6.1	3	0.5	233.9	338.7	475	481	6.1	0	0.0	446.9	356.0
225	231	6.1	2	0.3	239.5	336.6	481	487	6.1	2	0.3	445.5	362.0
231	237	6.1	0	0.0	245.6	334.3	487	493	6.1	20	3.3	443.9	367.9
237	243	6.1	2	0.3	251.7	332.2	493	499	6.1	13	2.1	442.0	373.8
243	249	6.1	1	0.2	256.6	330.4	499	505	6.1	8	1.3	441.6	379.9
249	256	6.1	9	1.5	262.7	328.0	505	511	6.1	2	0.3	440.7	385.7
256	259	3	8	2.7	268.7	325.9	511	518	6.1	4	0.7	439.8	391.9
259	262	3	115	38.3	271.4	324.8	518	524	6.1	3	0.5	439.0	397.9
262	268	6.1	20	3.3	274.3	323.7	524	530	6.1	25	4.1	438.2	404.0
268	274	6.1	70	11.4	279.6	321.4	**Average vents per m =4.7**					**Max = 38.3**	
							Standard Deviation = 4.8					**Min = 0**	

Table 3: CO2 Gas vent outflow volume measurements and estimations. Areas are based on Figure 9. Locations are in meters from the temporary bench mark (N4118002.47, E298647.54 UTM).

Sample ID	Volume (Liters)	Time (sec)	Discharge rate (L/Sec)	Number of vents of similar size	Gas outflow (L/sec)	Approximate location East (X)	North (Y)		Measured Volume	Estimated Volume
								Area One		0.06
GV9	0.5	24	0.02	25	0.52	115.8	399.3	Area Two	1.15	
GV10	0.5	20	0.03	25	0.63	70.1	424.6			
								Area Three		0.2
GV6	2.25	135	0.02	50	0.83	318.8	306.0	Area Four	2.18	
GV7	2.25	30	0.08	15	1.13	308.8	308.8			
GV8	0.5	45	0.01	20	0.22	281.6	331.3			
GV5	0.5	240	0.00	30	0.06	338.3	296.9	Area Five	0.06	
GV1	0.5	160	3.E-03	20	0.06	441.0	324.9	Area Six	1.01	
GV2	0.5	23	0.02	2	0.04	421.1	299.8			
GV3	0.5	60	0.01	60	0.50	390.1	295.7			
GV4	0.5	75	0.01	60	0.40	390.8	295.7			
								Area Seven		0.2
								Total estimated gas volume		**4.85**

Table 4: Solute Compositions of the Pah Tempe springs and Virgin River waters in Timpoweap Canyon. Sample # refers to the number in Figure 10. TDS is Total dissolved solids; Cond. is specific conductivity; upstream refers to Virgin River samples upstream of the Pah Tempe springs, downstream refers to samples below the springs

Sample Information		Hydrologic Parameters			Solute Composition														Error Balance			TDS (mg/L) (sum of cations and anions	Si
					Ca		Mg		Na		K		HCO3		Cl		SO4						
Sample #	BYU Lab ID	pH	Temp. (°C)	Cond. (µS)	mg/L	meq/L	mg/L	meq/L	mg/L	meq/L	mg/L	meq/L	mg/L	meq/L	mg/L	meq/L	mg/L	meq/L	Cations	Anions	% Error		ppm
Virgin River																							
1	2742	8.4		769	64.8	3.2	28.1	2.3	47.6	2.1	4.8	0.12	232	3.8	46.8	1.3	114.38	2.4	7.7	7.5	1.4	424.06	
2	2747	8.4		770	67.6	3.4	28.7	2.4	49.2	2.1	5.0	0.13	244	4.0	48.2	1.4	119.2	2.5	8.0	7.9	0.9	442.64	
3	2740	8.3	13.6	651	71.5	3.6	28.2	2.3	20.5	0.9	3.6	0.09	218	3.6	16.1	0.5	127.09	2.7	6.9	6.7	1.4	357.91	
4	2741	8.6	7	786	64.0	3.2	28.7	2.4	52.3	2.3	4.9	0.13	227	3.7	56.2	1.6	148.29	3.1	7.7	8.4	2.9	433.11	
5	2743	6.6	34.4	1237	676.6	33.8	132.0	10.9	2477	107.8	204.3	5.23	1143	18.7	3029	85.5	1890	39.4	158	144	4.7	7662	
6	2744	6.6	31.6	1258	665.2	33.2	132.6	10.9	2430	105.7	201.9	5.16	1141	18.7	3116	87.9	1900	39.6	155	146	2.9	7687	
Average VR upstream		**8.4**	**10.3**	**744**	**66.9**	**3.3**	**28.4**	**2.3**	**42.4**	**1.8**	**4.6**	**0.12**	**230.25**	**3.8**	**41.8**	**1.2**	**127.24**	**2.7**	**7.6**	**7.6**	**1.7**	**414.4**	
Average VR downstream		**6.6**	**33**	**1248**	**670.9**	**33.5**	**132.3**	**10.9**	**2453.5**	**106.7**	**203.1**	**5.20**	**1142**	**18.7**	**3073**	**86.7**	**1895**	**39.5**	**156**	**145**	**4**	**7674**	
Springs																							
7	2746	6.3	40.6	1461	725.2	36.2	140.3	11.6	2809	122.2	226.3	5.79	1268	20.8	3585	101.1	1974	41.1	175.73	163.01	3.8	8753.6	
8	2739	6.1	40.9	1452	734.8	36.7	140.3	11.6	2793	121.5	228.4	5.84	1279	21.0	3562	100.5	1822	37.9	175.57	159.39	4.8	8737	23.0
9	2745	6.3	39.4	1461	707.0	35.3	139.0	11.4	2796	121.6	225.7	5.77	1273	20.9	3536	99.7	2022	42.1	174.13	162.7	3.4	8676	22.7
10	3628	6.4	40	1430	741.4	37.0	145.0	11.9	2099	91.3	194.8	5.0	1258	20.6	3476	98.1	1466	30.5	145	149	1.4	7914	24.4
11	3629	6.4	40	1430	768.4	38.3	151.9	12.5	2105	91.6	223.0	5.7	1306	21.4	3818	107.7	1632	34.0	148	163	4.8	8373	24.1
Average Spring Water		**6.3**	**40.2**	**1447**	**735.4**	**36.7**	**143.3**	**11.8**	**2520**	**109.6**	**219.6**	**5.62**	**1277**	**20.9**	**3595**	**101.4**	**1783**	**37.1**	**164**	**159**	**3.6**	**8491**	**23.6**
Standard Deviation		**0.1**	**0.6**	**15.77**	**22.6**	**1.1**	**5.3**	**0.4**	**382**	**16.6**	**14.0**	**0.36**	**18**	**0.3**	**131**	**3.7**	**234**	**4.9**	**15.6**	**6.0**	**1.4**	**357.2**	**0.8**

Table 5: Isotope Compostions of the Virgin River, springs and a gas sample in Timpoweap Canyon. Saturation indices for the Virgin River and springs calculated in WATEQ, postive is supersaturated,

	BYU Lab ID	Date	d18O (‰)	d2H (‰)	d13C (‰)	3H (TU)	Saturation indices (log SI) Gypsum	Calcite	Dolomite	Halite	Quartz
Virgin River											
1	2742	2/14/2002	-12.9	-95.7			-1.6	0.9	1.6	-7.2	
2	2747	2/14/2002					-1.6	0.9	1.6	-7.2	
3	2740	2/14/2002	-12.5	-93.2			-1.5	0.8	1.4	-8.0	
4	2741	2/14/2002	-13.0	-94.7			-1.5	0.9	1.6	-7.1	
5	2743	2/14/2002					-0.2	0.6	1.0	-3.9	
6	2744	2/14/2002	-13.1	-106.0			-0.2	0.6	0.9	-3.9	
Average Upstream VR			**-12.8**	**-94.5**			**-1.5**	**0.8**	**1.4**	**-7.3**	
Average Downstream VR			**-13.1**	**-106.0**			**-0.2**	**0.6**	**0.9**	**-3.9**	
Springs											
7	2746	2/14/2002	-13.0	-108.0			-0.2	0.4	0.7	-3.8	
8	2739	2/14/2002	-13.6	-108.3			-0.2	0.3	0.3	-3.8	0.4
9	2745	2/14/2002	-13.9	-107.7			-0.2	0.4	0.6	-3.8	1.0
10	3628	5/19/2004	-13.6	-108.7	-2.1	<0.2	-0.2	0.6	0.9	-3.9	0.4
11	3629	5/19/2004	-13.5	-108.5			-0.2	0.6	1.0	-3.9	0.4
12	3633	5/22/2003	-13.2	-108.3							
13	3632	5/22/2003	-13.2	-108.4							
14	3263	3/31/2003	-12.8	-105.9							
15	3262	3/31/2003	-12.9	-108.3							
16	3261	3/31/2003	-12.8	-108.3							
17	3260	3/31/2003	-13.1	-108.6							
18	3259	3/31/2003	-13.7	-107.4							
19	3258	3/31/2003	-12.7	-108.9							
20	3257	3/31/2003	-13.0	-108.6							
21	3256	3/31/2003	-13.1	-108.2							
22	3255	3/31/2003	-13.6	-108.5							
23	3254	3/31/2003	-12.8	-108.4							
Average spring water			**-13.2**	**-108.2**	**-2.1**	**<0.2**	**-2.0**	**0.5**	**0.7**	**-3.8**	**0.4**
Standard Deviation			**0.4**	**0.7**							
Gas Vent											
Pah Tempe gas											
	21272	4/3/2003	27.1		-5.3						

Table 6: Fracture analysis in the field. Density units are m/m^2. Locations are shown in Figure 13 and are in meters from the temporary bench mark (N4118002.47, E298647.54 UTM).

South Canyon Wall					North Canyon Wall				
Name	**North**	**East**	**Elevation**	**Density**	**Name**	**North**	**East**	**Elevation**	**Density**
FR-20	1087.3	664.9		4.62	FR-1	1623.8	-152.3	124.0	4.00
FR-21	1069.0	704.1		3.75	FR-2	1559.5	-27.4	112.7	0.00
FR-22	1098.9	712.9		2.67	FR-3	1512.6	70.2		2.45
FR-23	1031.3	813.4		6.82	FR-4	1484.9	87.7		0.00
FR-24	1030.7	818.6		7.50	FR-5	1435.5	290.4		4.53
FR-25	1003.7	908.5		5.24	FR-6	1394.8	360.9		3.78
FR-26	997.3	926.6		5.04	FR-7	1394.8	377.9		5.49
FR-27	979.5	977.6		9.44	FR-8	1326.4	552.8		1.06
FR-28	972.0	998.2		2.50	FR-9	1311.5	600.2		1.65
FR-29	971.0	1001.0		2.67	FR-10	1270.5	702.3		3.75
FR-30	970.0	1004.0		3.52	FR-11	1254.2	753.0		3.15
FR-31	968.5	1012.6		6.97	FR-12	1193.0	869.6		4.52
FR-32	963.2	1029.2		4.83	FR-13	1173.3	914.5		1.71
FR-33	959.5	1039.0		3.96	FR-14	1173.3	925.5		4.37
FR-34	959.0	1045.0		5.05	FR-15	1153.9	937.3		4.40
FR-35	958.5	1048.0		6.08	FR-16	1140.7	1009.6		8.14
FR-36	959.5	1045.3	101.8	5.16	FR-17	1120.1	1041.2		4.79
FR-37	955.6	1068.1	103.4	4.97	FR-18	1120.1	1060.2		0.56
FR-38	958.8	1080.2	96.3	7.03	FR-19	1120.1	1088.2		0.94
FR-39	956.2	1095.9	91.4	7.34					
FR-40	943.4	1113.1	91.9	3.34					
FR-41	929.2	1125.5	93.2	5.07					
FR-42	925.9	1168.6		3.69					
FR-43	924.0	1194.7		2.74					
FR-44	928.0	1205.7		3.32					
FR-45	935.9	1228.5	96.5	2.80					
FR-46	945.0	1251.0		4.34					
FR-47	953.0	1271.6	95.4	2.91					
FR-48	955.6	1281.0		4.01					
FR-49	955.9	1283.7		4.60					
FR-50	956.8	1286.4		3.20					
FR-51	968.0	1337.0		2.10					
FR-52	975.0	1366.0		2.03					
FR-53	980.0	1381.0		2.91					
FR-54	982.8	1386.8	95.4	3.07					
FR-55	983.0	1389.5		5.42					
FR-56	987.0	1404.5		3.62					
FR-57	987.9	1407.9	102.0	5.91					
FR-58	994.4	1438.6	119.1	4.55					
FR-59	995.6	1441.0	119.7	5.14					
FR-60	1015.4	1482.9	133.9	5.62					
FR-61	1026.0	1500.1	140.5	4.09					
FR-62	1051.1	1520.6	140.2	4.09					
FR-63	1070.2	1525.2	138.3	3.73					
FR-64	1107.9	1564.7	151.6	4.07					
FR-65	1127.2	1586.7	154.0	4.42					

For both canyon walls	
Mean density	4.08
Standard Deviatio	1.85
Maximum	9.44
Minimum	0.00

Table 7: Fracture analysis from the photo mosaic of the southern canyon wall in Timpoweap Canyon (Figure 17).

Name	Distance from fault (m)	Density (m/m^2)
CR1	439	1.77
CR2	436	1.17
CR3	432	2.00
CR4	428	0.87
CR5	421	2.03
CR6	416	0.70
CR7	412	1.59
CR8	407	1.04
CR9	403	0.93
CR10	398	1.04
CR11	394	0.77
CR12	390	0.51
CR13	385	0.94
CR14	381	1.27
CR15	377	1.06
CR16	372	0.87
CR17	367	0.54
CR18	362	0.72
CR19	356	1.34
CR20	352	1.05
CR21	348	0.65
CR22	344	0.70
CR23	341	1.38
CR24	337	1.22
CR25	333	1.11
CR26	329	1.11
CR27	325	1.47
CR28	321	2.03
CR29	317	1.84
CR30	313	1.94
CR31	309	2.06
CR32	306	1.58
CR33	303	0.66
CR34	299	1.78
CR35	295	0.83
CR36	291	1.37
CR37	287	1.24
CR38	284	0.06
CR39	280	0.60
CR40	276	1.69
CR41	272	1.37
CR42	268	0.75
CR43	264	0.60
CR44	260	0.34
CR45	253	1.24
CR46	245	0.79
CR47	238	0.90
CR48	236	2.21
CR49	235	1.05
CR50	233	1.51
CR51	231	2.04
CR52	229	1.55
CR53	228	1.77
CR54	226	2.30
CR55	224	2.45
CR56	223	1.28
CR57	221	1.78
CR58	219	1.60
CR59	213	0.76
CR60	206	1.27
CR61	200	1.80
CR62	194	1.19
CR63	187	2.38
CR64	181	1.03
CR65	175	1.25
CR66	169	1.49
CR67	164	0.52
CR68	160	0.77
CR69	156	1.11
CR70	151	1.21
CR71	147	0.78
CR72	142	0.66
CR73	138	0.74
CR74	133	0.91
CR75	129	0.61
CR76	125	0.58
CR77	120	1.63
CR78	113	1.49
CR79	106	1.25
CR80	98	0.66
CR81	91	1.69
CR82	84	0.91
CR83	77	0.66
CR84	69	1.47
CR85	62	1.50
CR86	55	0.96
Mean density		**1.21**
Standard Deviation		**0.51**
Maximum		**2.45**
Minimum		**0.06**

Table 8: Depth of circulation calculations for the Pah Tempe spring waters using the reported geothermal-gradient and spring discharge temperature, geothermomter temperatures, and possible groundwater temperatures based on stable isotopes.

Possible groundwater temperatures	Temp. (°C)	Mean air Temp. (°C)	Temperature difference (°C)	Range of depths (km) for the range of geothermal gradient (°C/km) 18.5	33.7
Mean spring discharge	40.2	16.1	24.1	1.30	0.72
Mean Conductive geothermometer	69.8	16.1	53.7	2.90	1.59
Mean Adiabatic geothermometer	74.5	16.1	58.4	3.16	1.73
Mean of conductive and adiabatic	72.1	16.1	56.0	3.03	1.66
δ18O and δ2H 100°C	100.0	16.1	83.9	4.54	2.49
δ18O and δ2H 125°C	125.0	16.1	108.9	5.89	3.23

Table 9: Geothermometer analysis (°C) of maximum temperatures of Pah Tempe Springs

Water Sample # (Table 4)	Water discharge temp.	Silica				
		Conductive	Adiabatic	Chalcedony	Cristobalite	Amorphous
8	41	69	74	37	19	-42
9	39	68	73	36	19	-42
10	40	71	76	39	22	-40
11	40	71	75	39	21	-40
Average	**40**	**70**	**75**	**38**	**20**	**-41**
Average Temp of conductive and adiabatic			**72**			

FIGURES

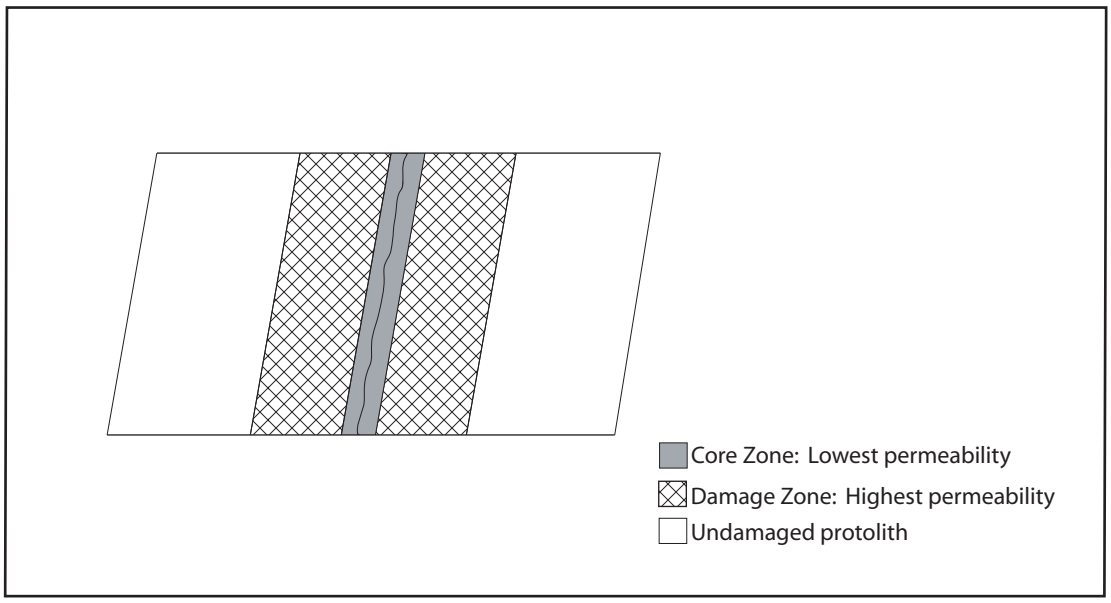

Figure 1: Generalized fault zone modified after Caine et. al. (1996). The Hurricane Fault in the area of Timpoweap Canyon has these hydraulic and structural elements.

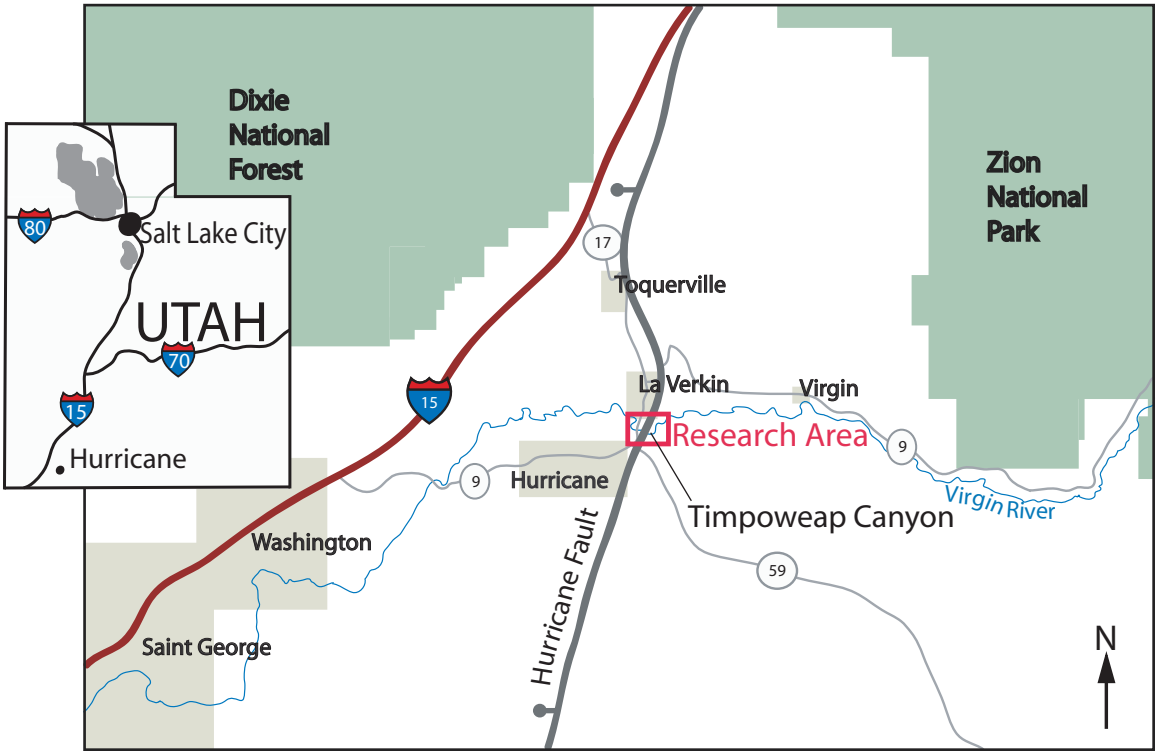

Figure 2: Index map of the research area in Timpoweap Canyon, Hurricane, Utah. The generalized location of the Hurricane Fault is also shown.

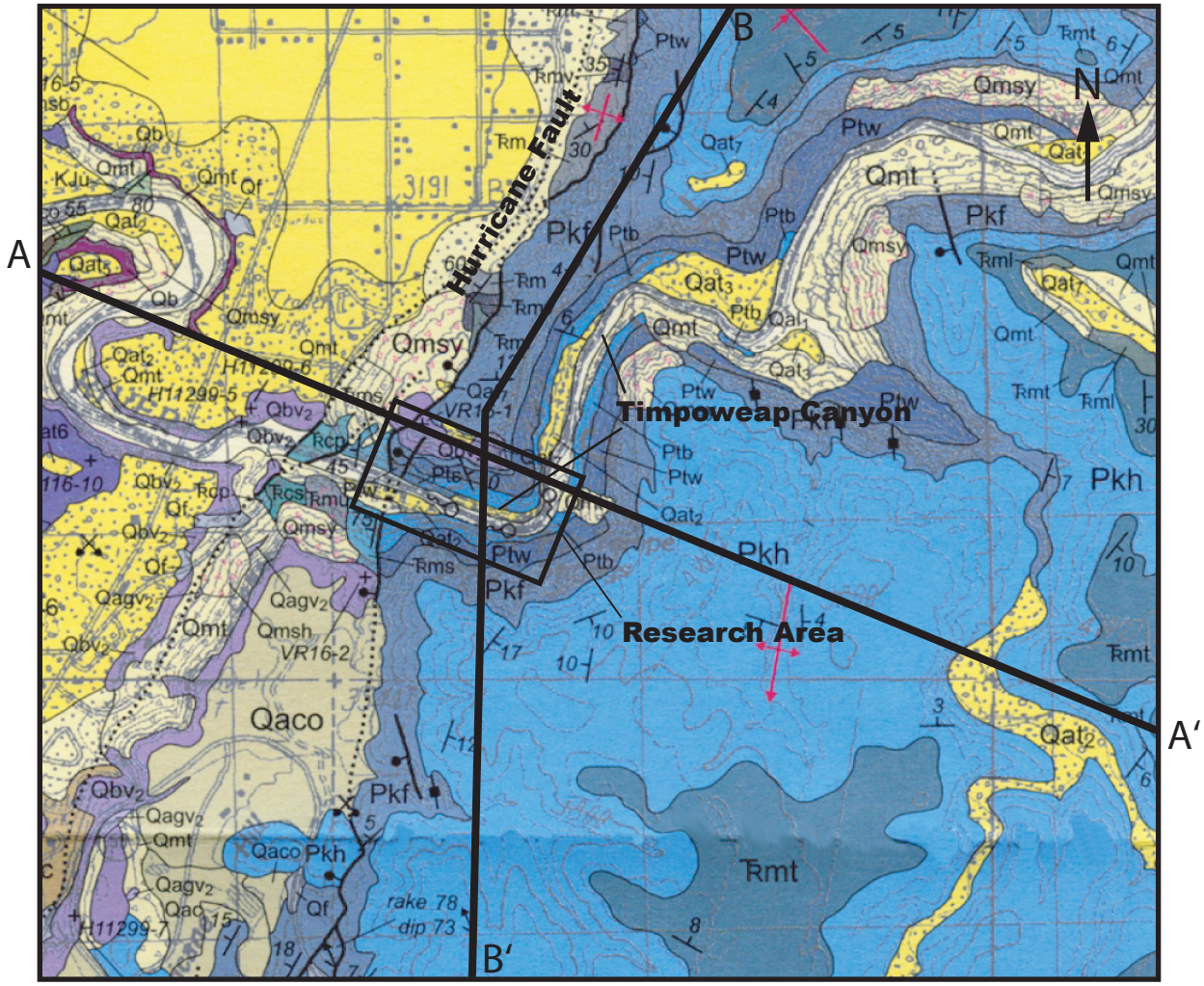

Figure 3: Geologic map of Timpoweap Canyon after Biek (2003). Location of cross-section A to A' and elevation profile B to B' are also indicated (Figure 4). Triassic and older rocks crop out in the footwall of the Hurricane Fault while Cretaceous to Triassic rocks crop out in the hanging wall.

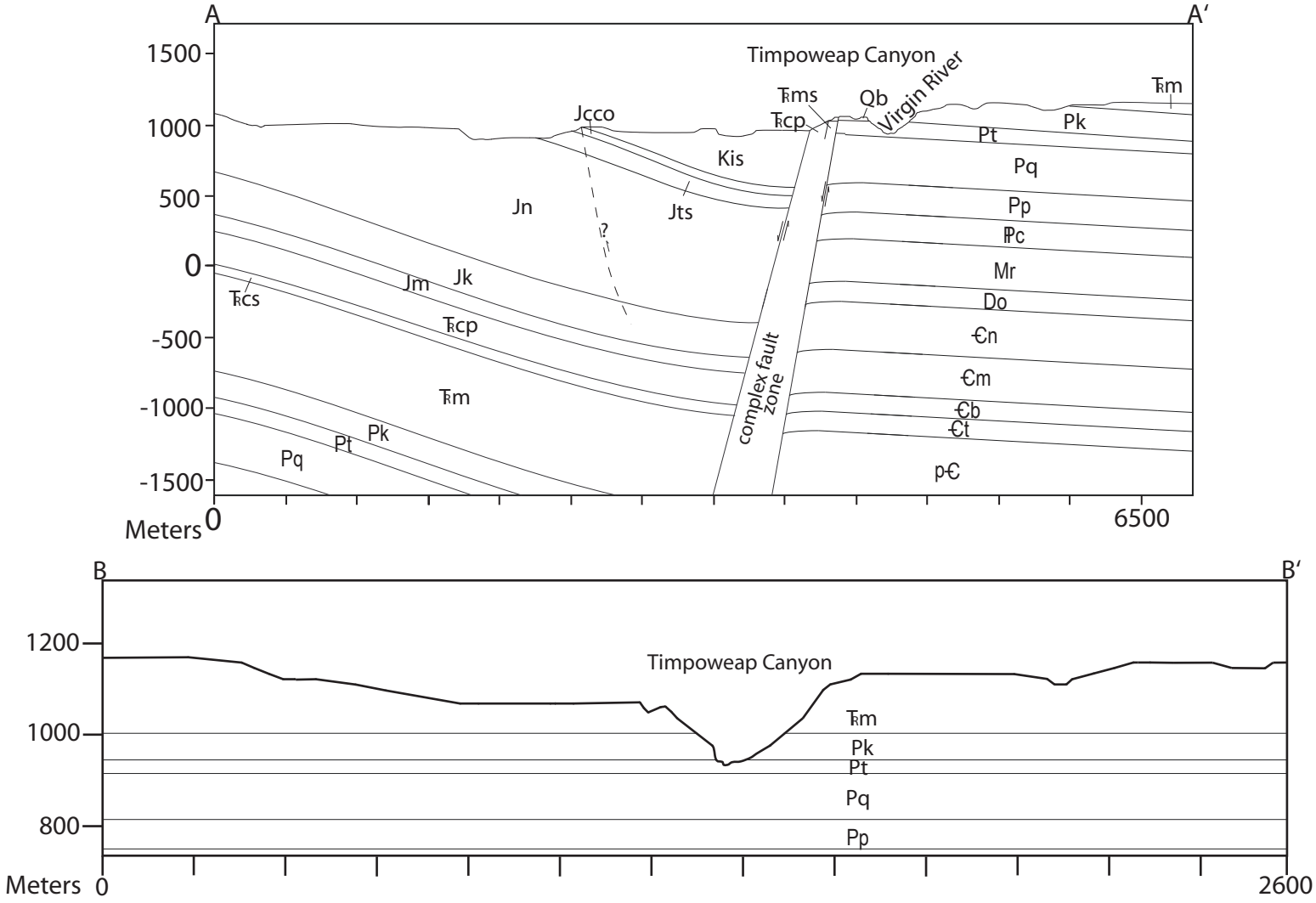

Figure 4: Cross-sections from A to A' and B to B' as shown in Figure 3. The cross-section was modified after Biek, 2003.

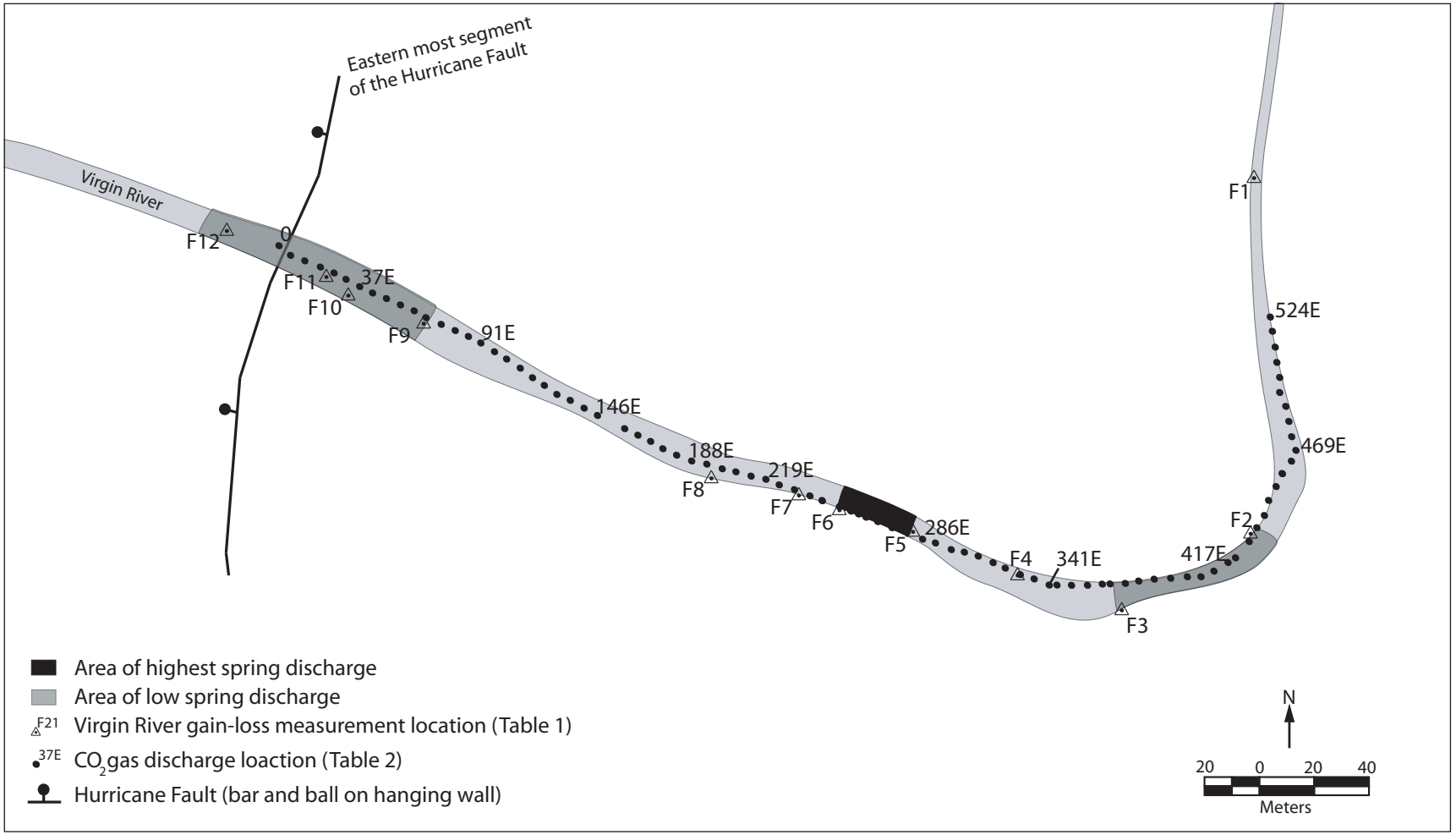

Figure 5: Index map of gain-loss measurements and CO_2 gas discharge locations of Timpoweap Canyon and areas of high and low spring discharge from Figure 7 (Gas vents are labeled by the distance in meters east from the fault).

Figure 6: Stratigraphic column of Timpoweap Canyon. The Pah Tempe Springs discharge from the Brady Canyon Member of the Toroweap Fm. The formations that crop out on the west of the Hurricane fault are Cretaceous or older (Figure 3 and 4). The formations on the footwall are Lower Triassic and older. The stratigraphic column was modified from Biek, 2003; Biek, 2000; Beus, 1987; Biek et. al., 2000; Harris, 1993; Hintze, 1988; and Langenheim, 1987.

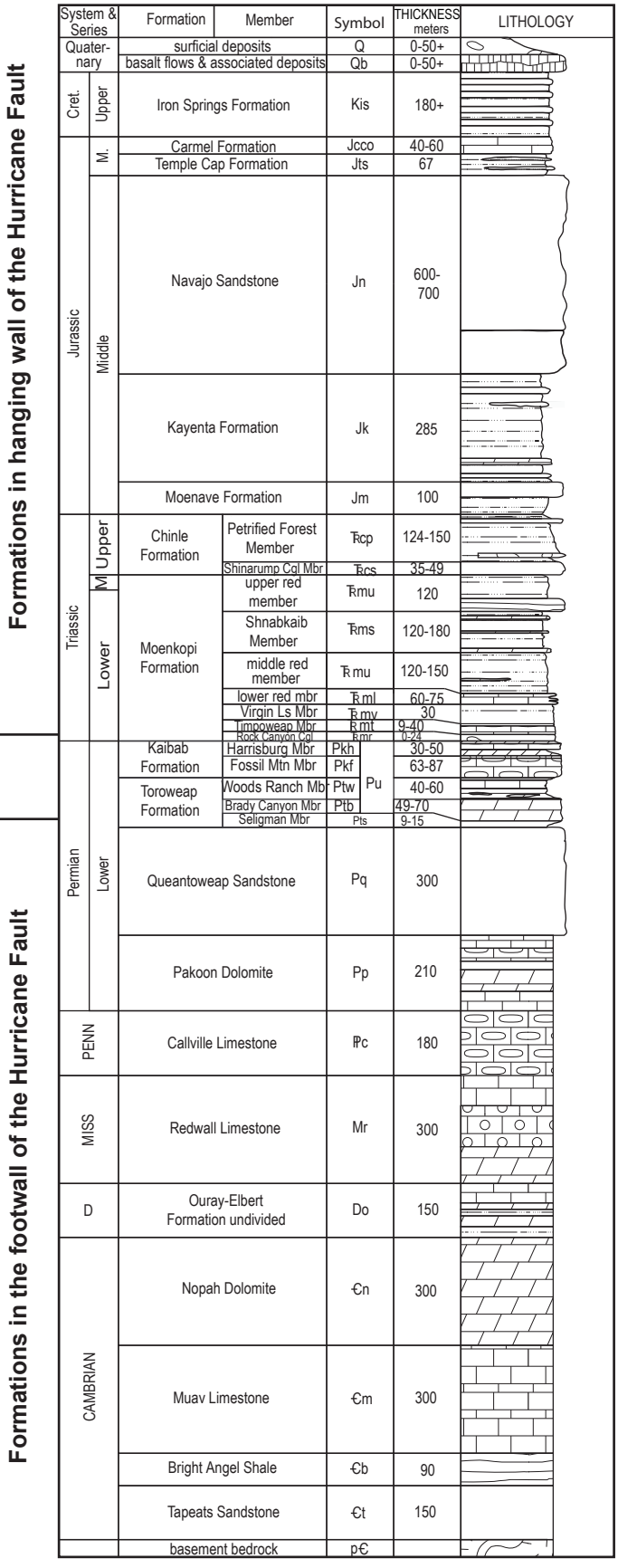

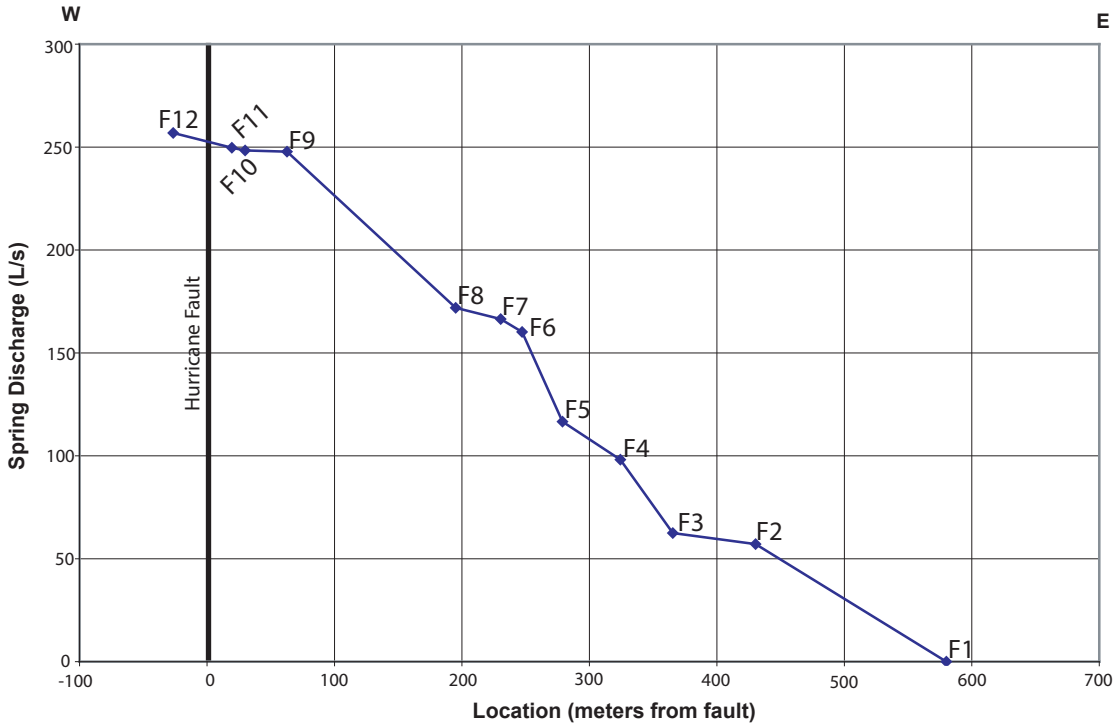

Figure 7: Cumulative Spring Discharge in Timpoweap Canyon in relation to distance from the Hurricane Fault.

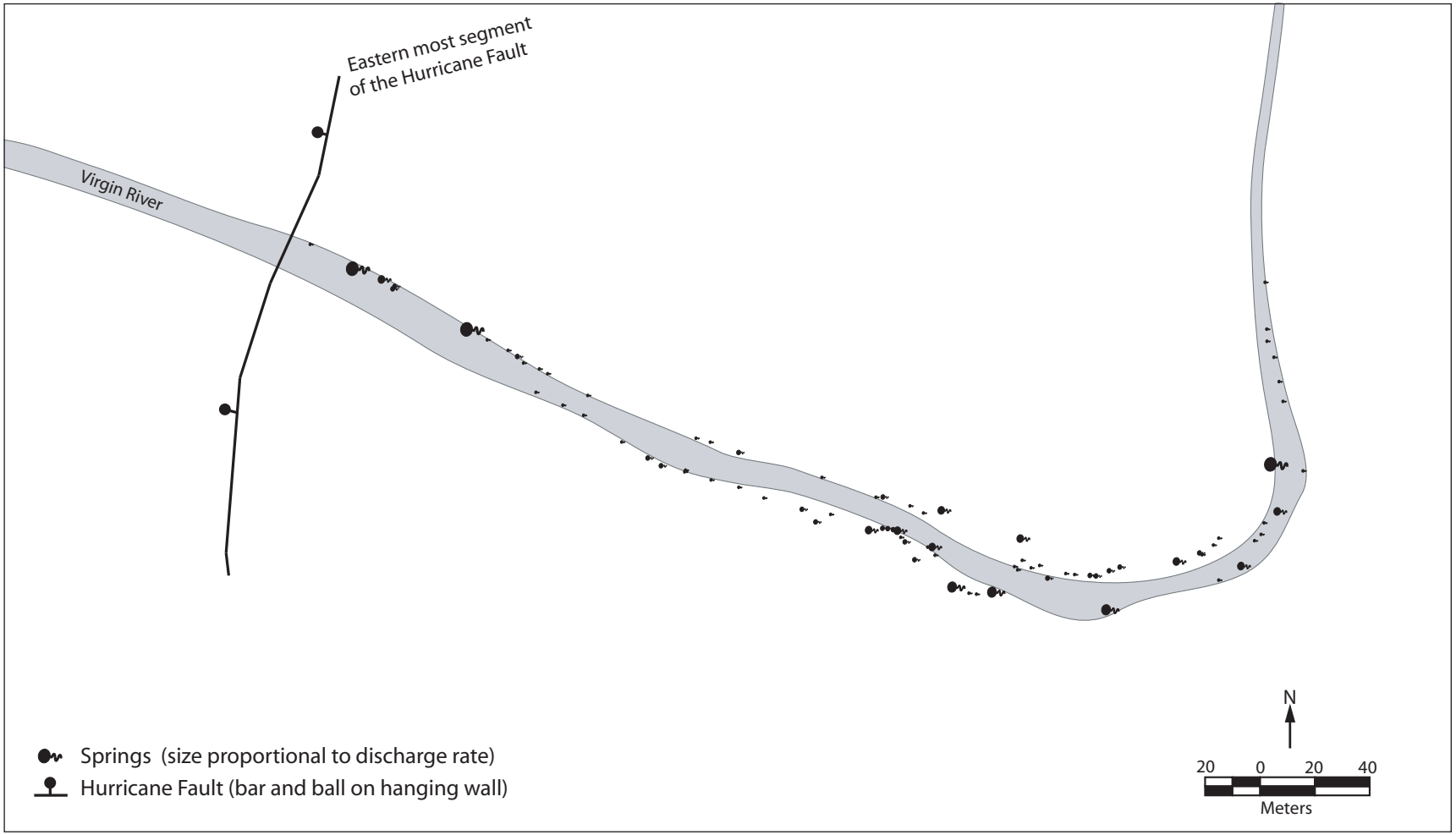

Figure 8: Index map of springs in Timpoweap Canyon. Springs are proportional to size, the discharge of the largest springs are estimated at 40-20 L/s.

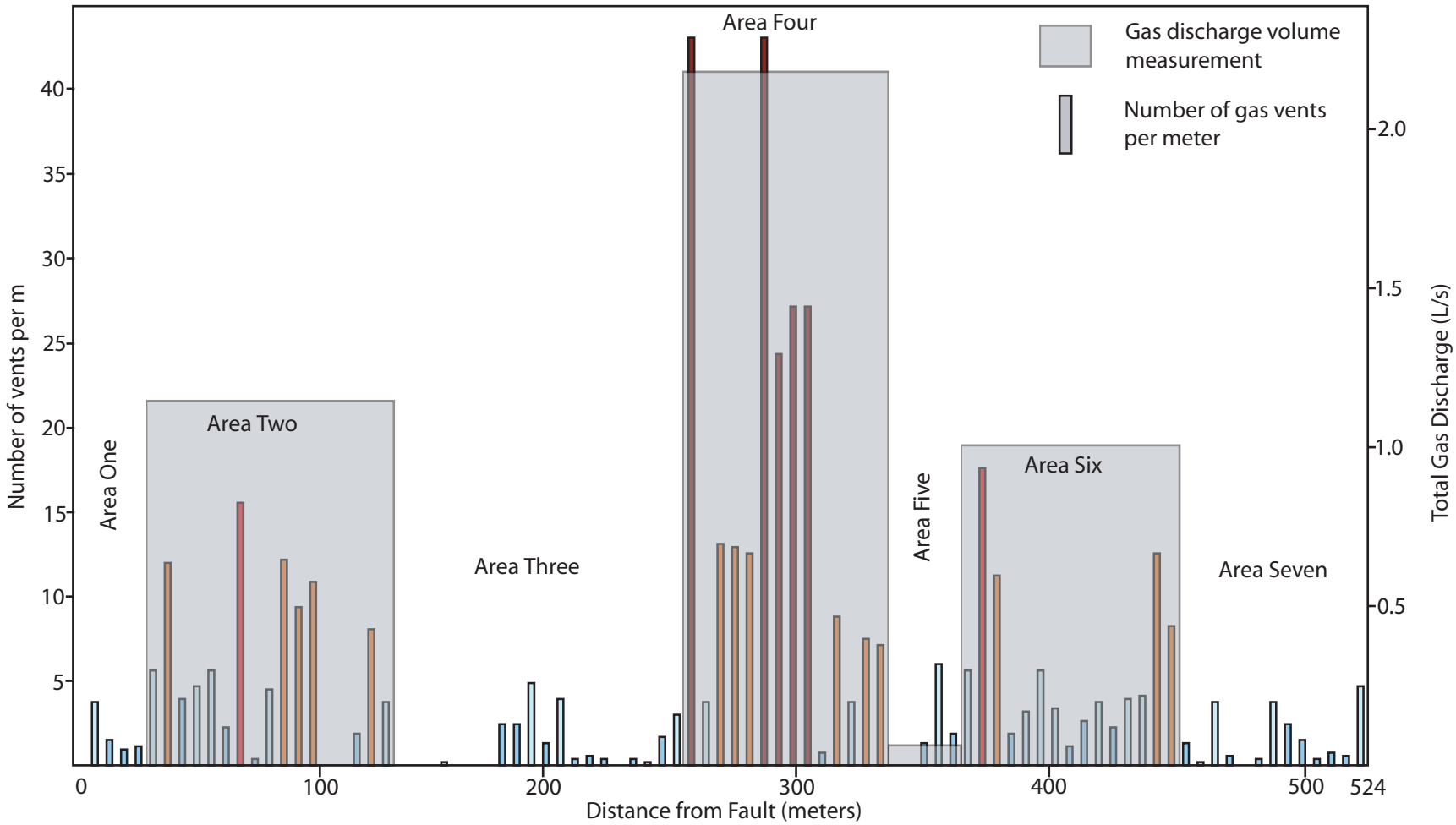

Figure 9: CO_2 Gas vent outflows along the Virgin River in Timpoweap Canyon occur in three significant areas of discharge. The volume of gas discharging in each area is represented by the larger gray reectangles and the axis on right.

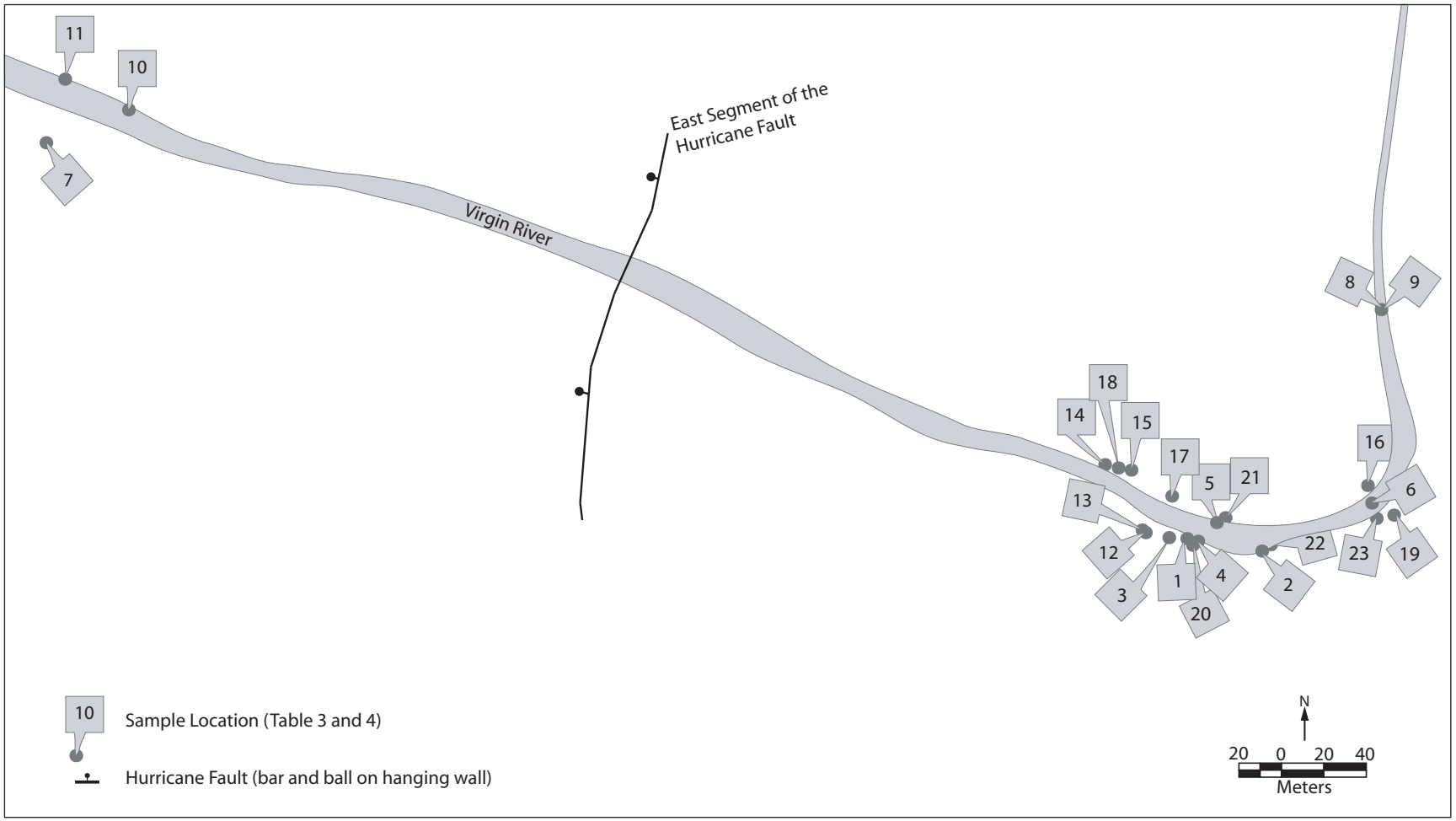

Figure 10: Index map showing locations of water samples collected in Timpoweap Canyon for solute composition and isotope analysis. Sample numbers correlate to Table 3 and 4. Samples 1-5 and 12-23 are samples of spring water. Samples 6-11 are samples of the Virgin River.

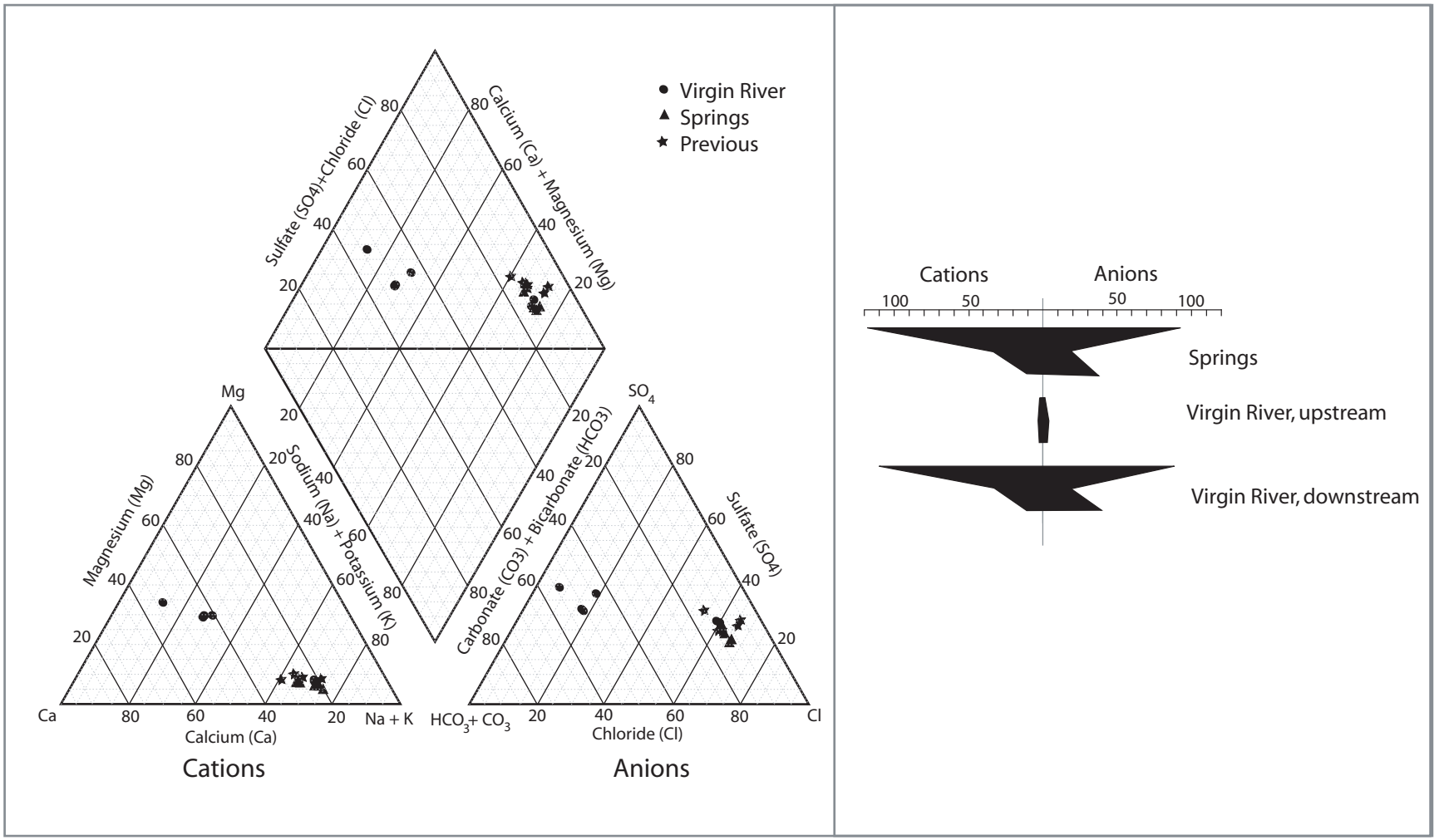

Figure 11: Piper plot and Stiff diagrams of the Pah Tempe Springs and Virgin River water in Timpoweap Canyon.

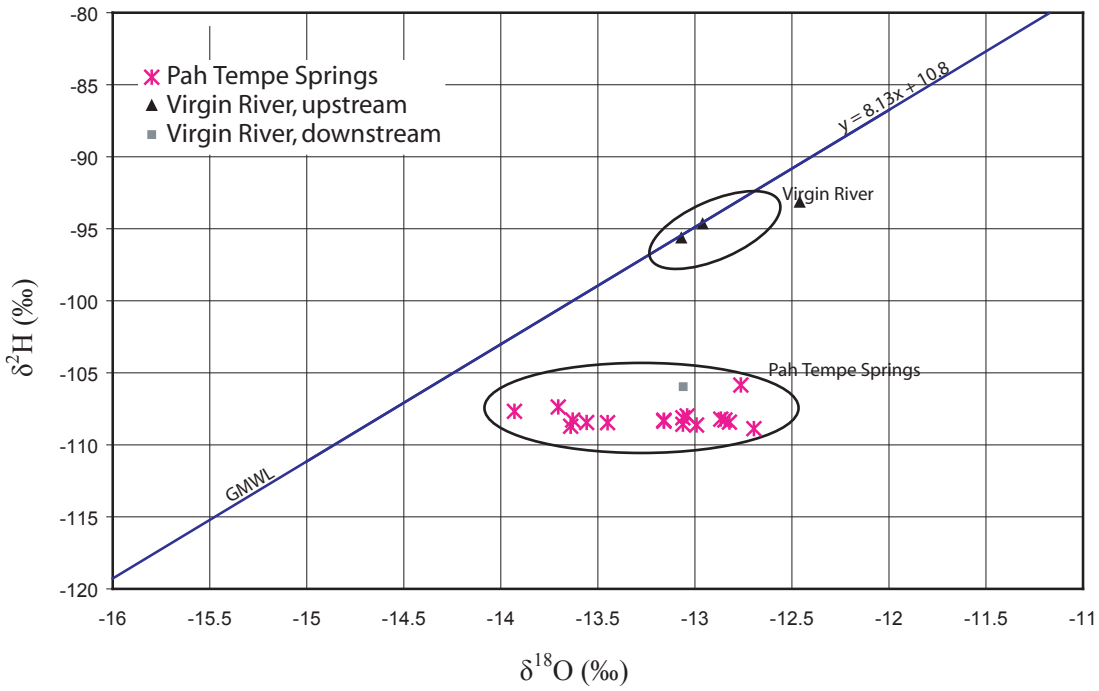

Figure 12: Stable isotopes, $\delta^{18}O$ and $\delta^{2}H$, plotted relative to the Global Meteoric Waterline (GMWL)

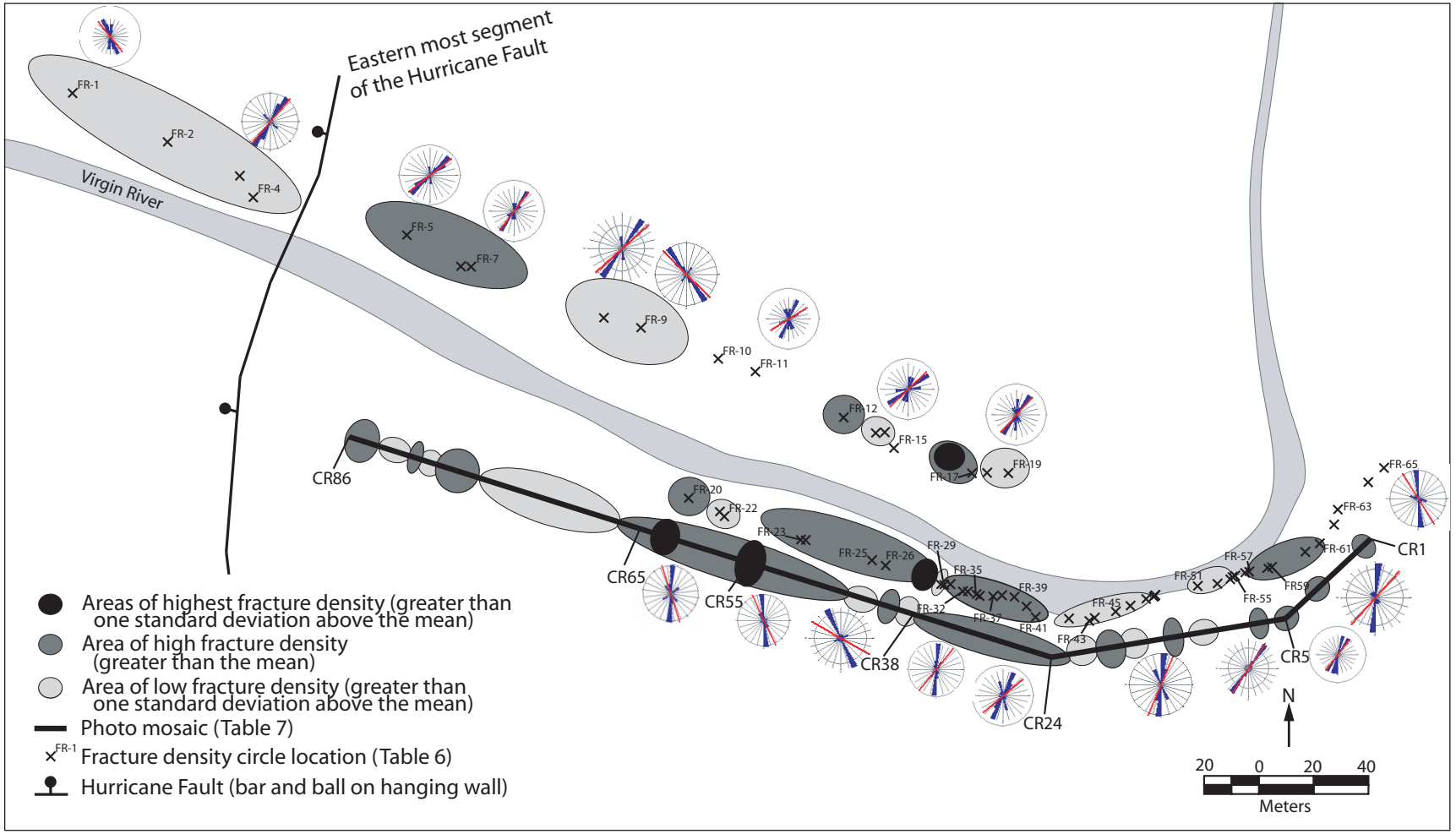

Figure 13: Index map of fracture analysis locations, including rose diagrams. The ellipses represent areas of high and low fracture density. The rose diagrams indicate a genreal trend parallel to the Hurricane Fault. Several locations of fracture density circles from the photo mosiac are labeled (i.e. CR86)

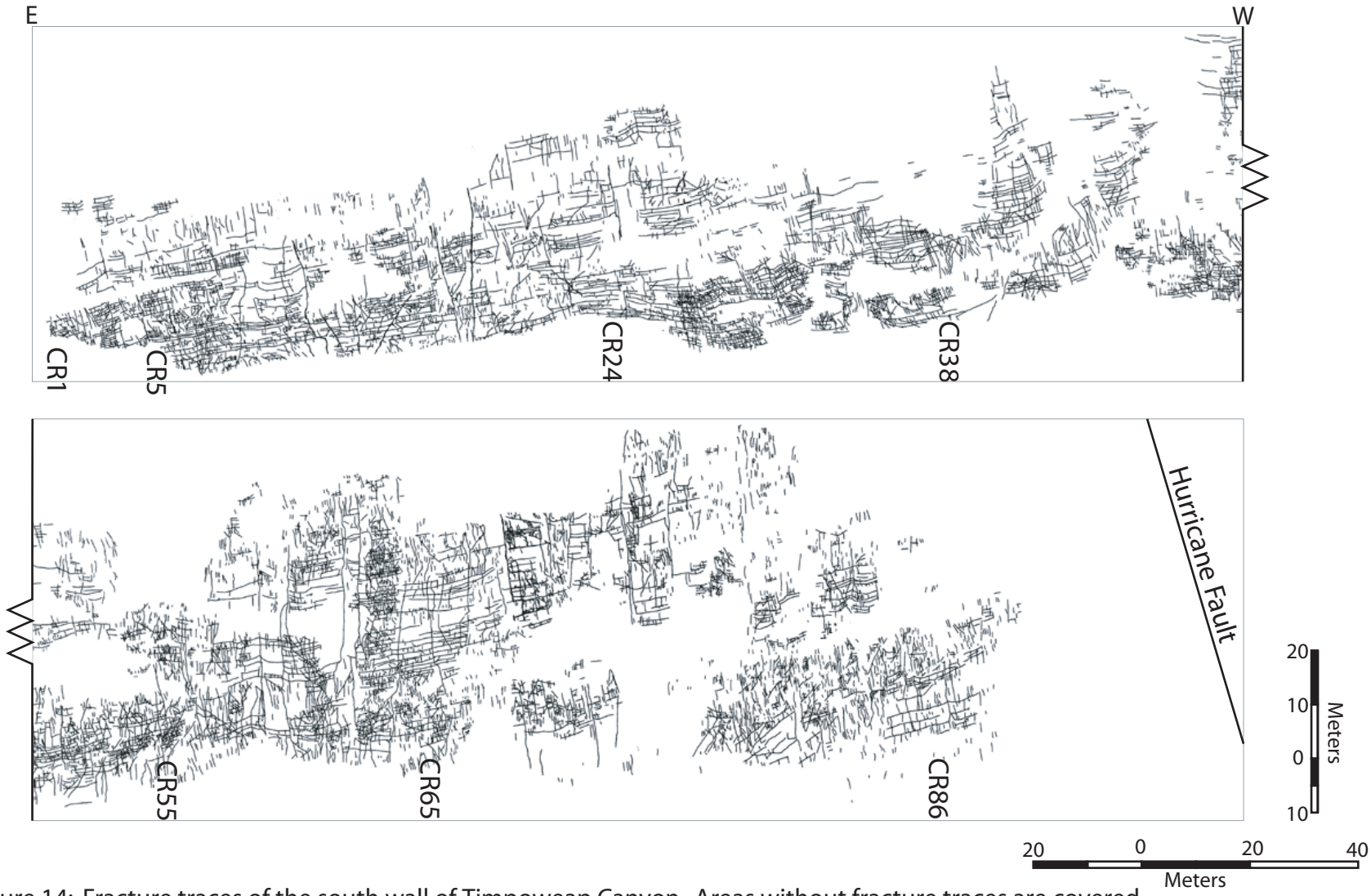

Figure 14: Fracture traces of the south wall of Timpoweap Canyon. Areas without fracture traces are covered by vegetation or talus slopes. Labels (i.e. CR55) are locations of fracture denisty analysis (Table 7, Figure 13)

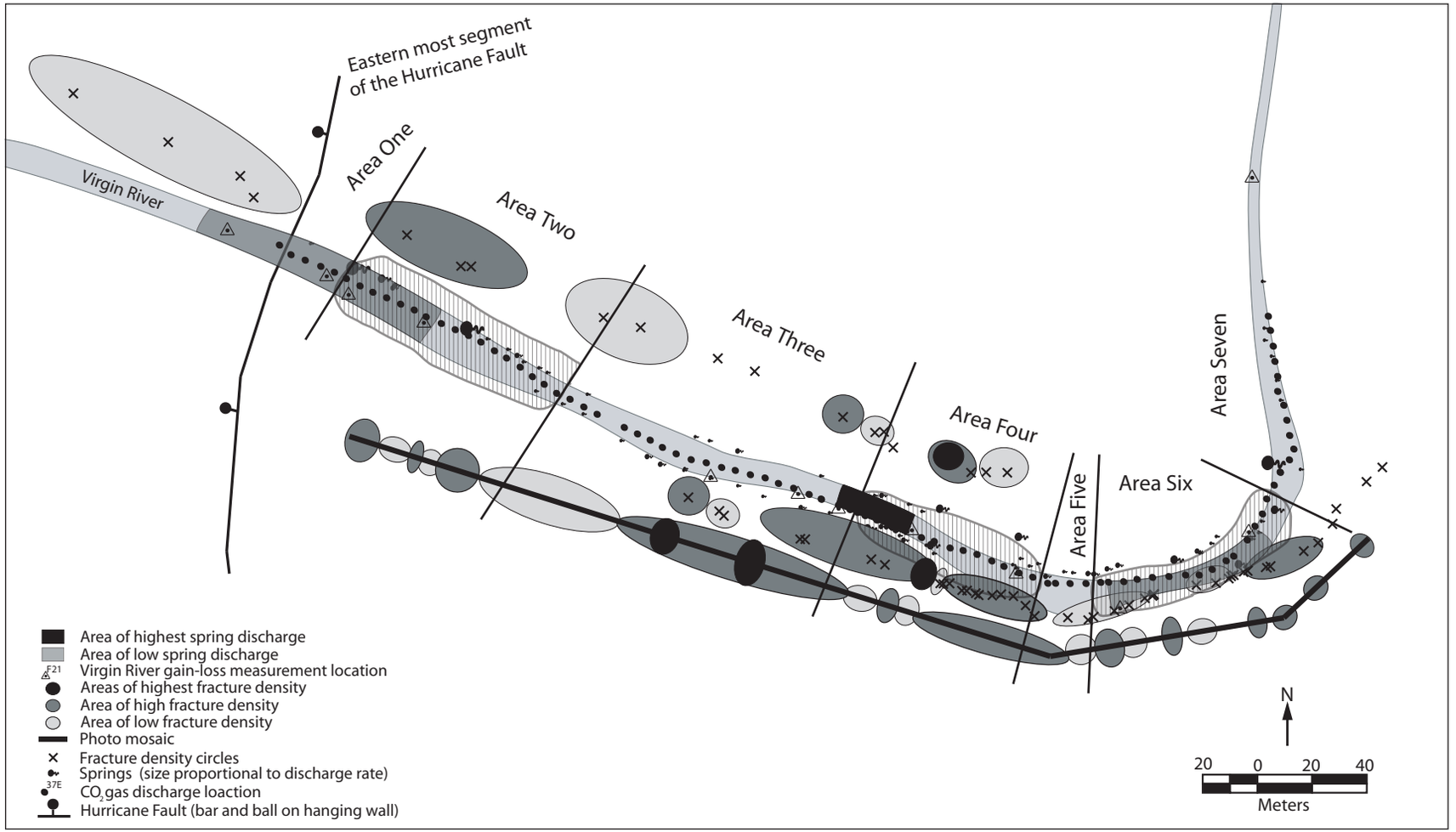

Figure 15: Areas from gas discharge (Figure 9) plotted against areas of high and low spring discharge, high and low fracture density, and locations of springs.

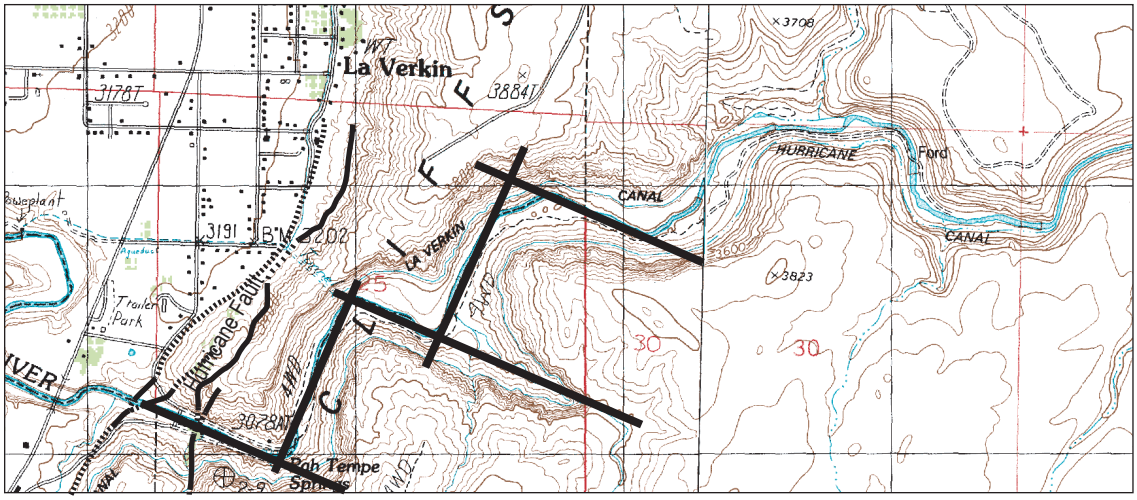

Figure16: The Virgin River follows a fracture pattern perpendicular to the Hurricane Fault

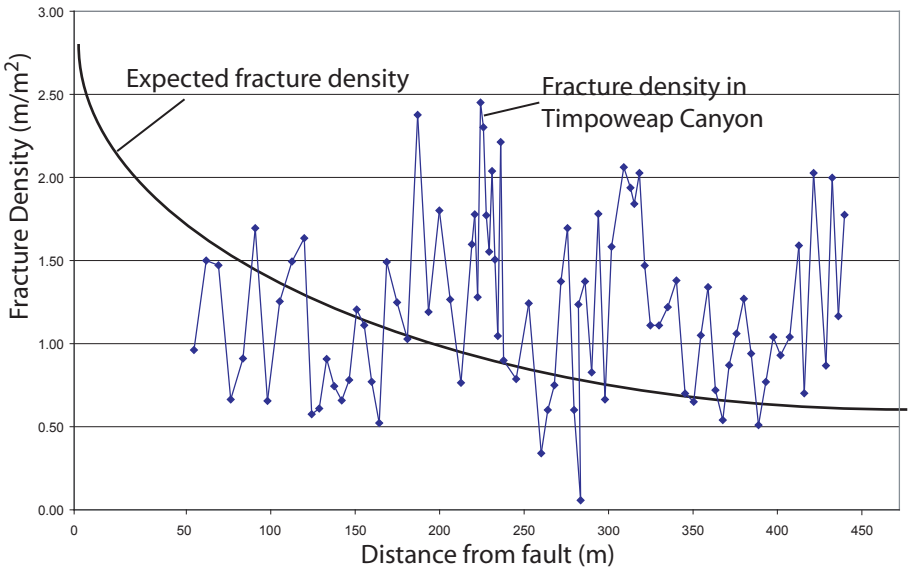

Figure 17: Fracture density pattern of the Timpoweap canyon compared to expected fracture pattern. The expected fracture density curve is based on a theoretical curve of an ideal fault.

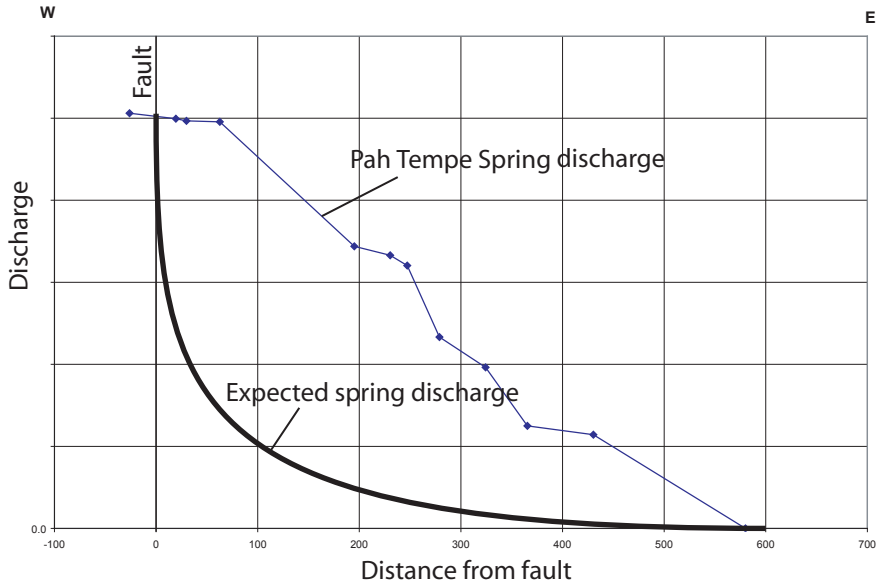

Figure 18: Spring dishcarge of the Virgin River compared to expected Spring Discharge. The expected spring discharge curve is based on a theoretical curve of an ideal fault.